RSC Advances

ROYAL SOCIETY OF CHEMISTRY

www.rsc.org/advances

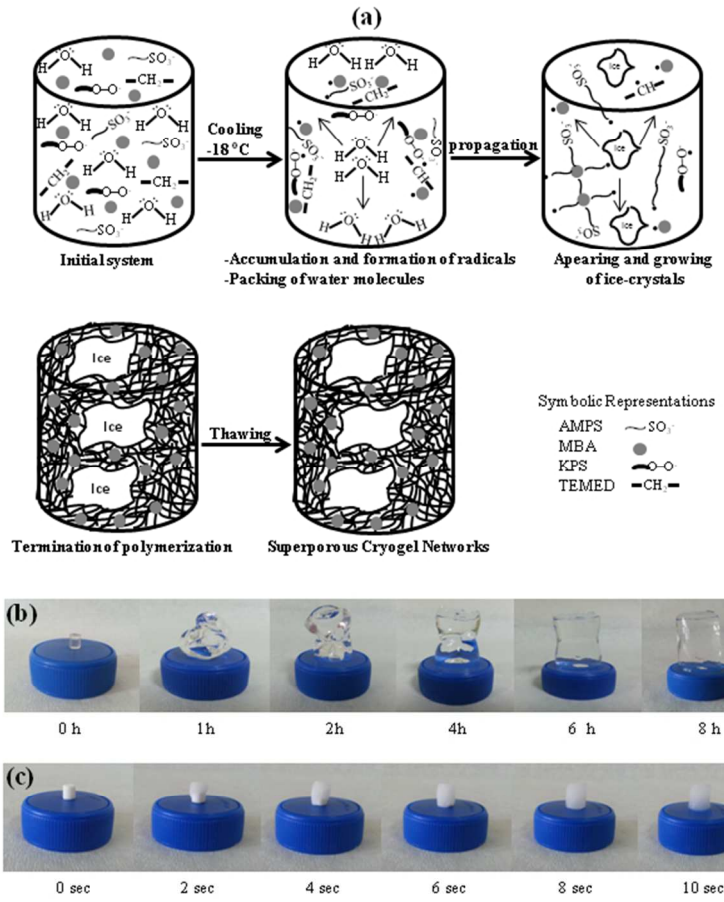

Figure 1. The polymerization mechanism of p(AMPS) cryogels **(a)**, and the visual demonstration of the swelling of 0.1% crosslinked p(AMPS) hydrogels **(b)**, and **(c)** 10% crosslinked p(AMPS) cryogels.

190x254mm (96 x 96 DPI)

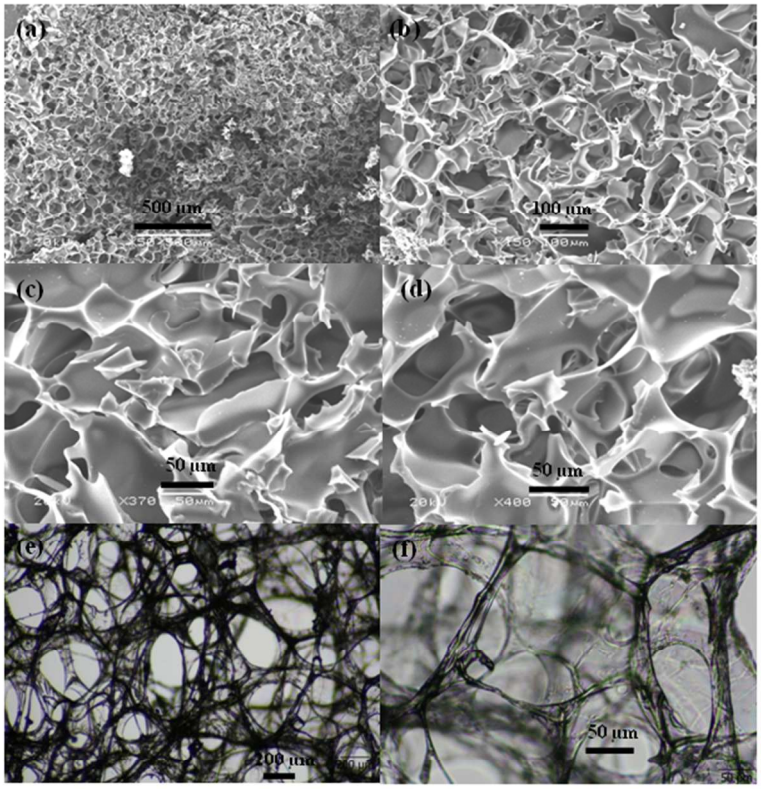

Figure 2. The SEM images of p(AMPS) cryogels under the **(a)** 50, **(b)** 150, **(c)** 370 and **(d)** 400 magnification and the optical microscope images of p(AMPS) cryogels under the **(e)** 10 and **(f)** 20 magnification.

190x254mm (96 x 96 DPI)

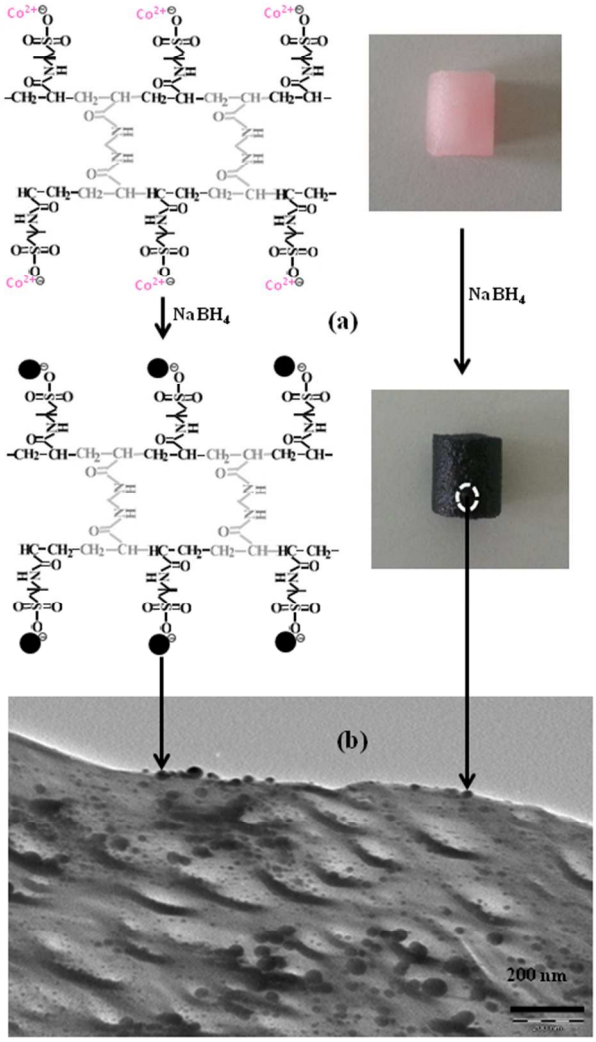

Figure 3. **(a)** The reduction of Co(II) ions to cobalt nanoparticles within cryogel matrices, and **(b)** TEM images of cobalt nanoparticles within porous cryogel networks.

190x254mm (96 x 96 DPI)

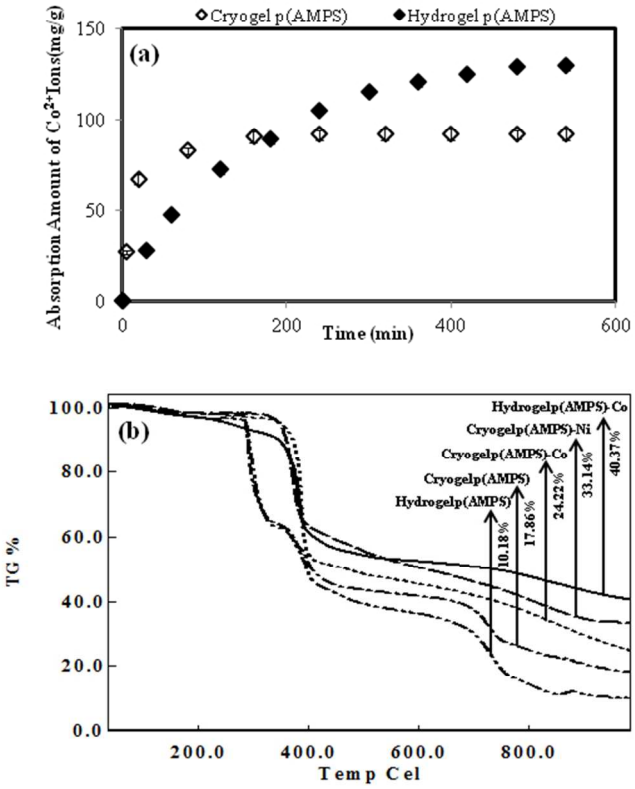

Figure 4. **(a)** Metal ion absorption capacities of p(AMPS) hydrogel and cryogel, and **(b)** TGA thermogram of p(AMPS) hydrogel, cryogel and their metal nanoparticle-containing composites.

190x254mm (96 x 96 DPI)

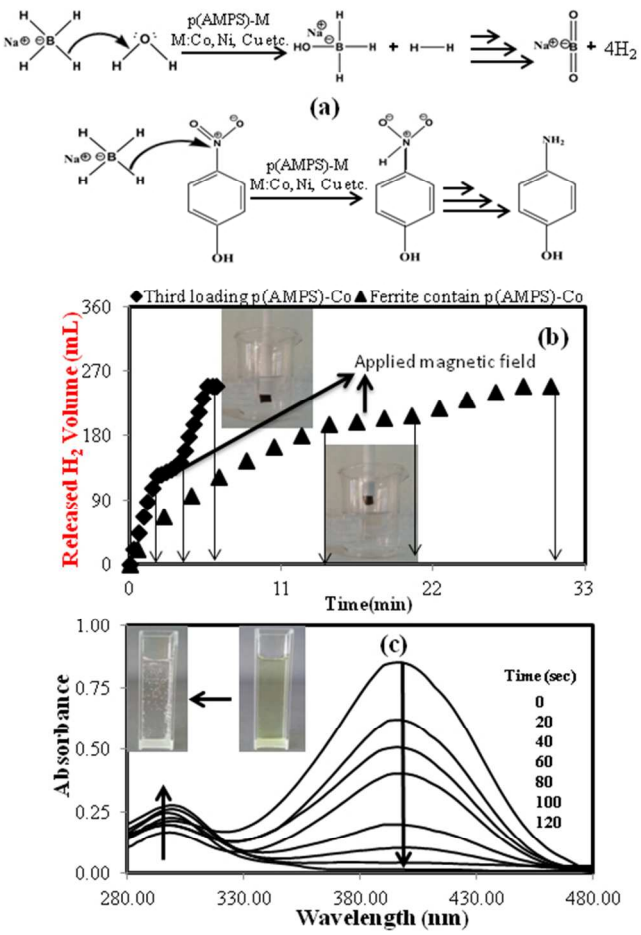

Figure 5. **(a)** Reaction mechanisms of H_2 generation from hydrolysis of $NaBH_4$, and reduction of 4-NP. **(b)** H_2 generation from hydrolysis of $NaBH_4$ via ferrite-containing 0.1 g p(AMPS)-Co metal nanoparticles (8.71 mg nanoparticles) and magnetic three times Co(II) loaded-reduced 0.1 g p(AMPS)-Co (19.54 mg/g nanoparticles) catalyst system under externally applied magnetic field. [Reaction conditions: 50 mL 50 mM $NaBH_4$, 5 wt% NaOH, 30 °C, 1000 rpm mixing rate.] **(c)** UV–Vis spectra of 4-NP reduction to 4-AP by using 0.1 g p(AMPS)-Co cryogel composite catalyst systems (8.62 mg Co nanoparticles) [Reaction conditions: 50 mL 0.01 M 4-NP, 0.28 M $NaBH_4$, 30 °C, 1000 rpm mixing rate].

190x254mm (96 x 96 DPI)

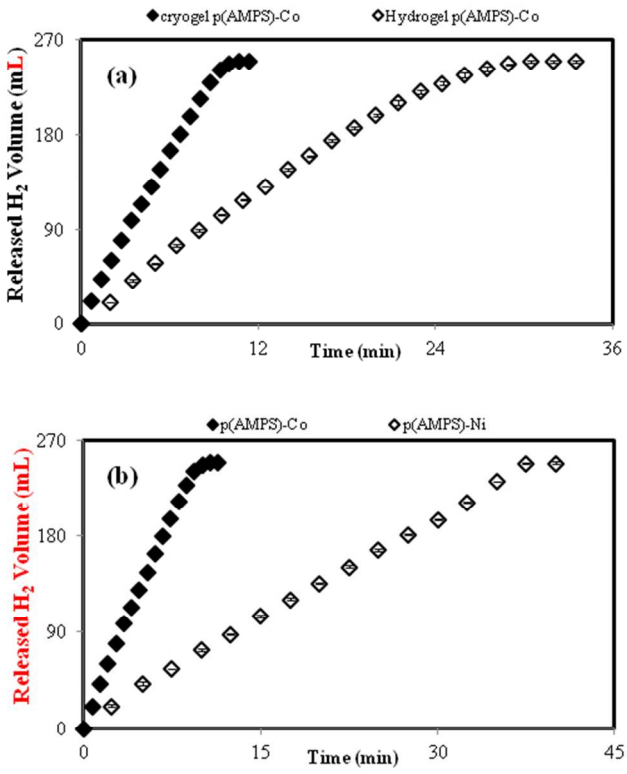

Figure 6. **(a)** H_2 generation from hydrolysis of 50 mL 50 mM $NaBH_4$ via 8.62 mg Co nanoparticle-containing 0.1 g cryogel p(AMPS)-Co composite, and 0.069 g hydrogel p(AMPS)-Co composites. [Reaction conditions: 50 mL 50 mM $NaBH_4$, 5 wt% NaOH, 30 °C, 1000 rpm.]
(b) H_2 generation from hydrolysis of $NaBH_4$ via 0.1 g cryogel p(AMPS)-Co (8.62 mg Co nanoparticles) and 0.1 g p(AMPS)-Ni composites (8.94 mg Ni nanoparticles). [Reaction conditions: 50 mL 50 mM $NaBH_4$, 5 wt% NaOH, 30 °C, 1000 rpm.]

190x254mm (96 x 96 DPI)

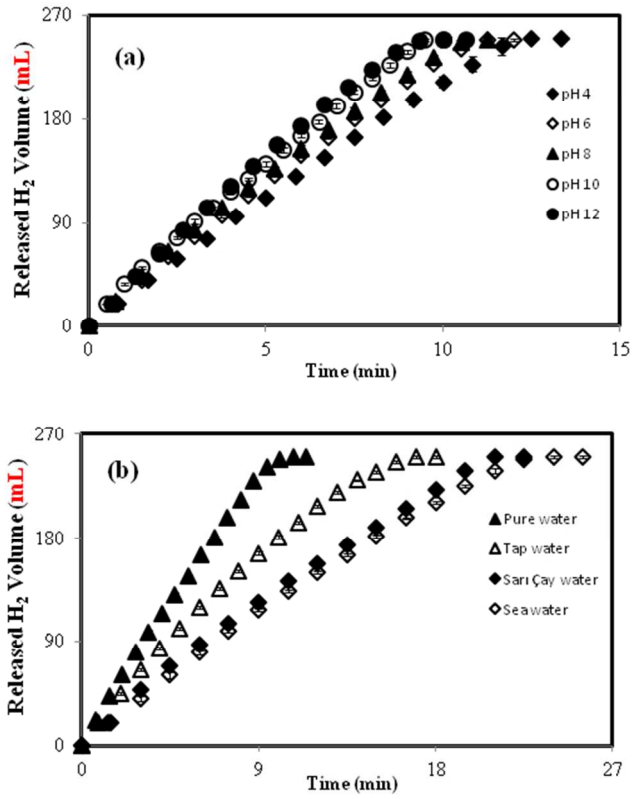

Figure 7. **(a)** The effect of pH and **(b)** the effect of water type on H_2 generation reaction from hydrolysis of sodium borohydride via 0.1 g cryogel p(AMPS)-Co (8.62 mg nanoparticles). [Reaction conditions: 50 mL 50 mM $NaBH_4$, 5 wt% NaOH, 30 °C, 1000 rpm].

190x254mm (96 x 96 DPI)

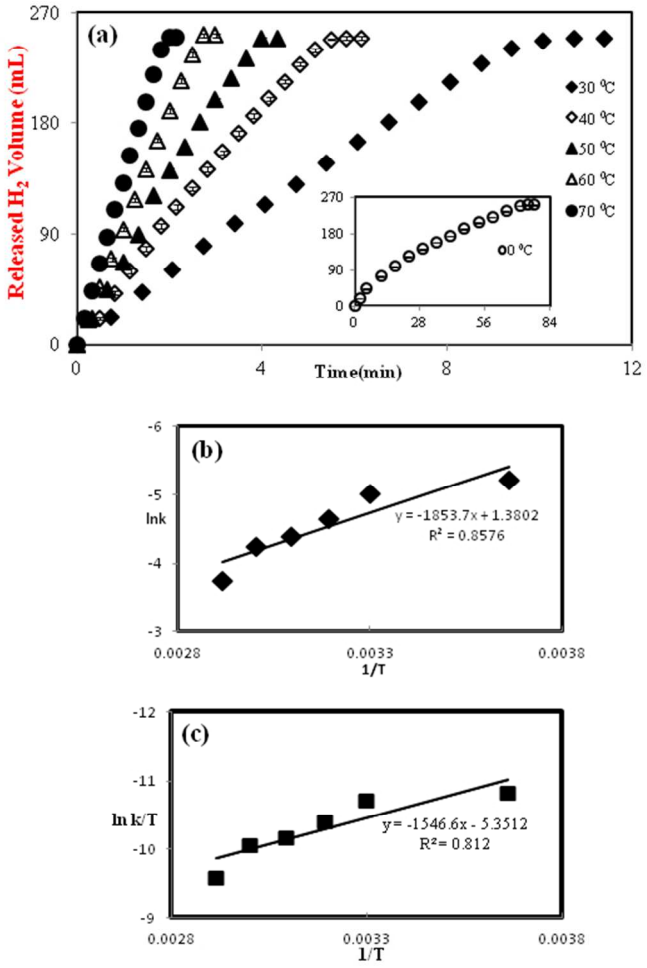

Figure 8. **(a)** The effect of temperature on the hydrolysis of $NaBH_4$, **(b)**, ln k versus 1/T (Arrhenius eq.), and **(c)**, ln (k/T) versus 1/T (Eyring eq.) [Reaction Conditions: 50 mL 50 mM $NaBH_4$, 5 wt% NaOH, 1000 rpm, 8.62 mg Co nanoparticles in 0.1 g cryogel p(AMPS)-Co composite].

190x254mm (96 x 96 DPI)

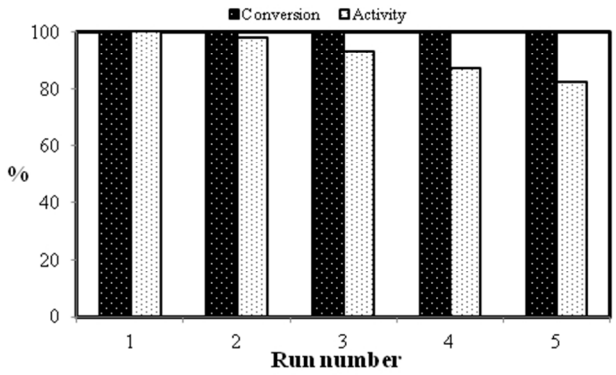

Figure 9. The activity and the conversion ability of the cryogel p(AMPS)-Co composite for repetitive $NaBH_4$ hydrolysis [Reaction conditions: 50 mL 50 Mm $NaBH_4$, 5 wt% NaOH, 30 °C, 1000 rpm, 8.62 mg Co nanoparticle in 0.1 g cryogel].

190x254mm (96 x 96 DPI)

Table 1. The amount of metal nanoparticles, TGA results, TOF (turn over frequency) values and hydrogen generation rates (HGR) of various catalyst systems.

Metal Ccomposites	**[a]Amount of Metal Nanoparticles**	**Weight loss % by TGA (%) at 1000 °C**	**[b]TOF**	**[c]HGR**
Hydrogel p(AMPS)-Co	124.88±1	40.37	2.24±0.2	950.90±0.3
Cryogel p(AMPS)-Co	86.27±1.2	24.22	6.37±0.1	2697.91±0.5
Cryogel p(AMPS)-Ni	89.41±1.5	33.14	1.64±0.12	699.11±0.2
3rd loading p(AMPS)-Co	195.42±1	53.11	6.25±0.1	2648.92±0.2
Magnetic p(AMPS)-Co	87.16±1.2	57.45	2.75±0.3	1171.54±0.1

[a]The amount of metal nanoparticles within cryogel/hydrogel as mg/g determined by AAS measurements.
[b]TOF (Total Turnover Frequencies) [(mol H_2) (mol catalyst min)$^{-1}$]
[c]HGR (Hydrogen Generation Rate) [(mL H_2) (min)$^{-1}$ (g of M)$^{-1}$]
Reaction Conditions: 50 ml 50 mM $NaBH_4$, 5% NaOH, 1000 rpm, 30 ^{0}C

Table 2. The change in TOF and HGR values of cryogel p(AMPS)-Co metal composites (8.62 mg particles) depending on different reaction conditions.

Change in TOF and HGR values with temperature, pH, reuse and the types of reaction water											
T(^{0}C)	**TOF**	**HGR**	**pH**	**TOF**	**HGR**	**Reuse**	**TOF**	**HGR**	**Water**	**TOF**	**HGR**
0±2	0.89±0.5	376.65±1.2	4	5.47±0.8	2320.18±1.5	1st	6.37±0.5	2697.91±0.5	DI	6.37±0.4	2697.91±1
40±1	11.74±0.8	4974.66±1	6	5.70±1.2	2416.86±1.2	2nd	6.32±0.7	2677.96±1.1	Tap	4.04±0.7	1706.01±1.2
50±1	17.12±1	7250.58±1.5	8	6.08±0.5	2577.98±1	3rd	5.87±0.5	2487.33±1.6	Sarı çay	3.26±0.3	1381.06±1.5
60±1	24.90±1	10546.29±1	10	6.22±1	2636.57±0.8	4th	5.47±1	2320.18±1.5	Sea	3.03±0.5	1288.99±1.3
70±1	34.25±1.2	14501.16±1	12	6.63±0.6	2807.58±1	5th	5.26±1	2230.95±1.2			

TOF (Total Turnover Frequencies) [(mol H_2) (mol catalyst min)$^{-1}$]
HGR (Hydrogen Generation Rate) [(mL H_2) (min)$^{-1}$ (g of M)$^{-1}$]

Graphical Abstract

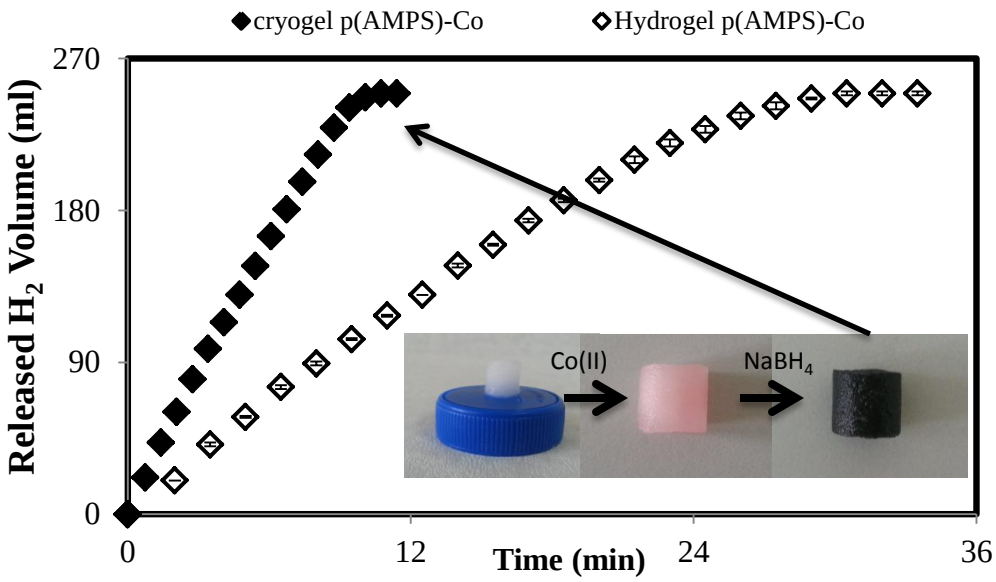

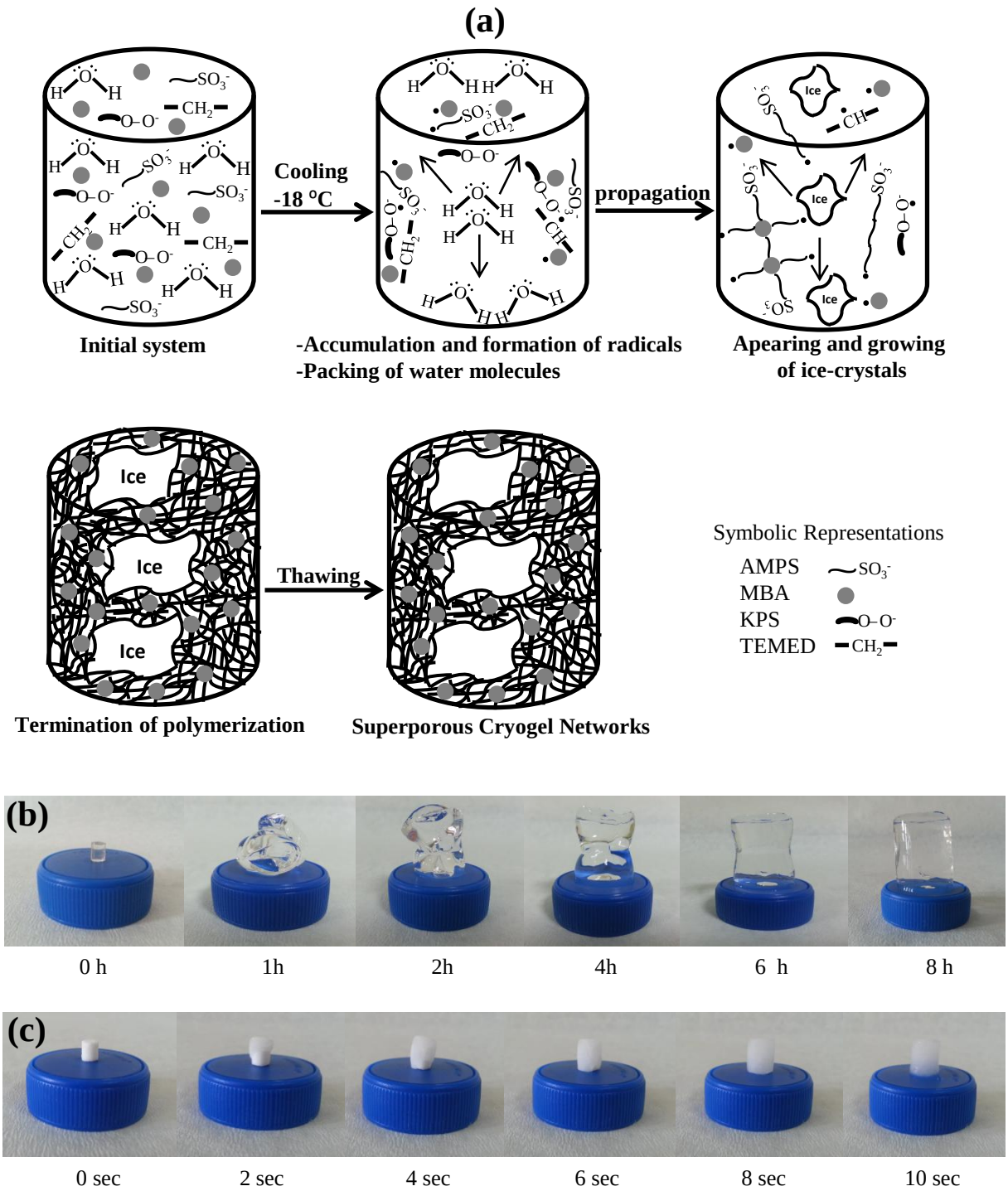

Figure 1. The polymerization mechanism of p(AMPS) cryogels **(a)**, and the visual demonstration of the swelling of 0.1% crosslinked p(AMPS) hydrogels **(b)**, and **(c)** 10% crosslinked p(AMPS) cryogels.

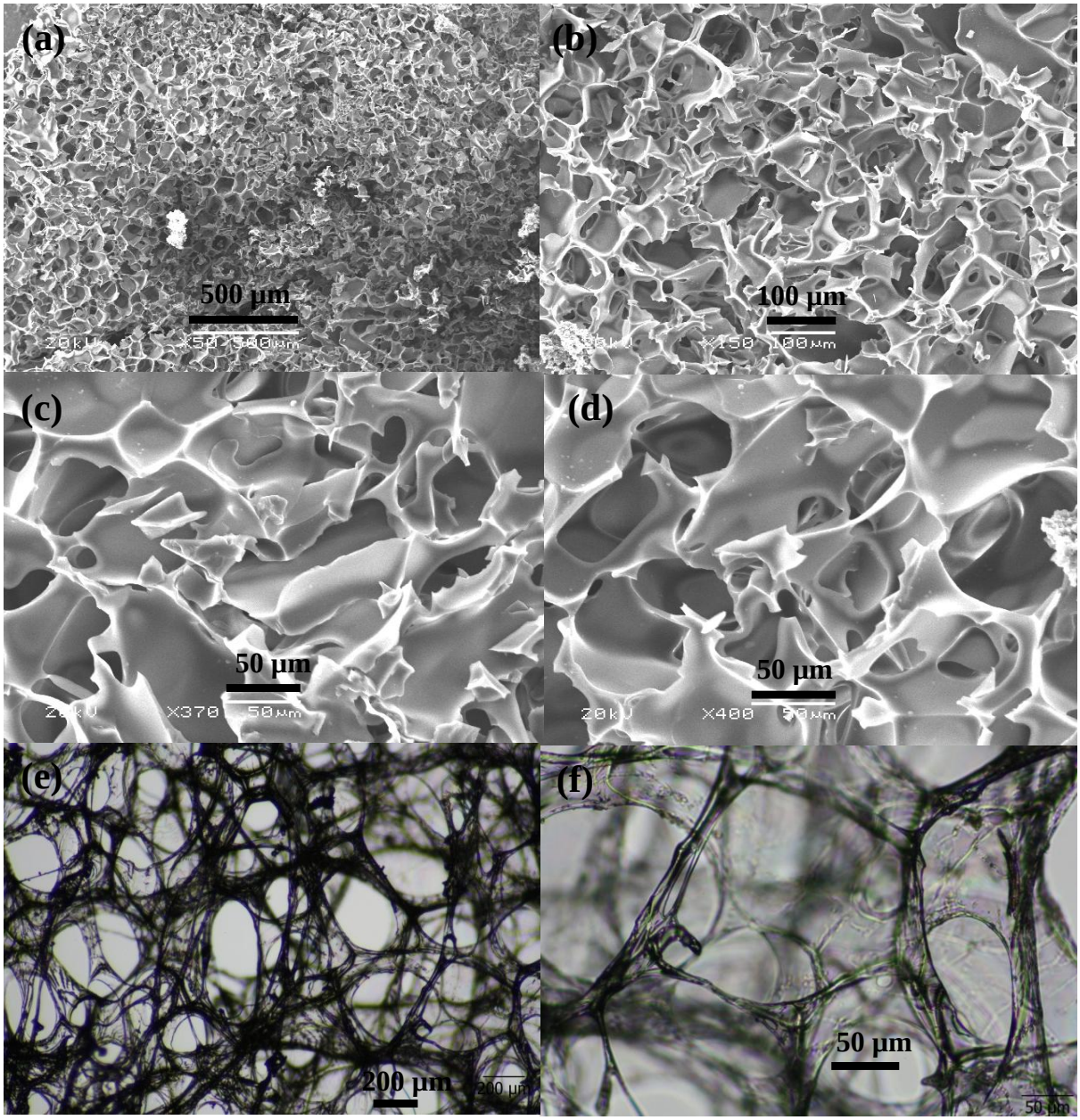

Figure 2. The SEM images of p(AMPS) cryogels under the **(a)** 50, **(b)** 150, **(c)** 370 and **(d)** 400 magnification and the optical microscope images of p(AMPS) cryogels under the **(e)** 10 and **(f)** 20 magnification.

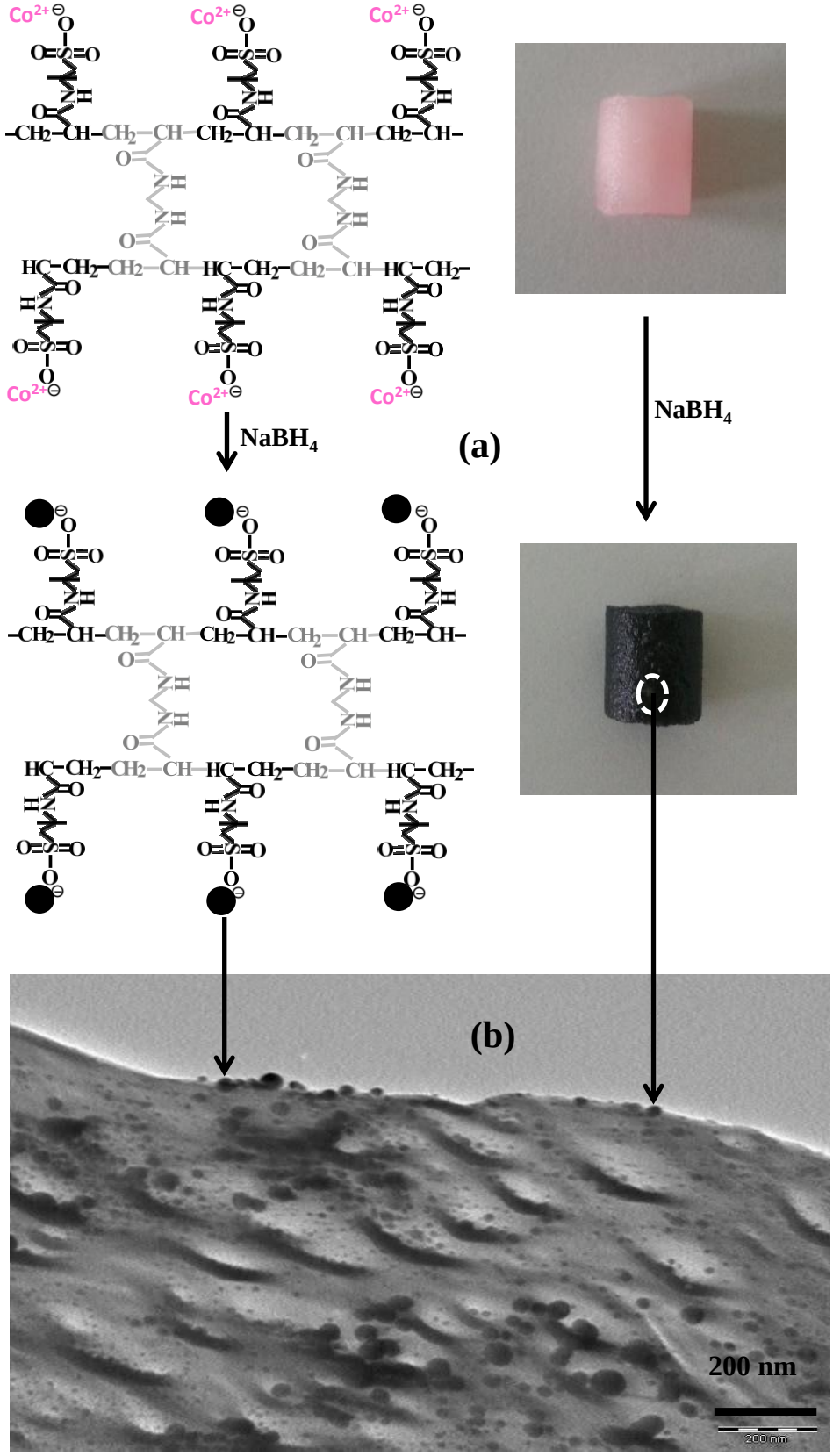

Figure 3. (a) The reduction of Co(II) ions to cobalt nanoparticles within cryogel matrices, and **(b)** TEM images of cobalt nanoparticles within porous cryogel networks.

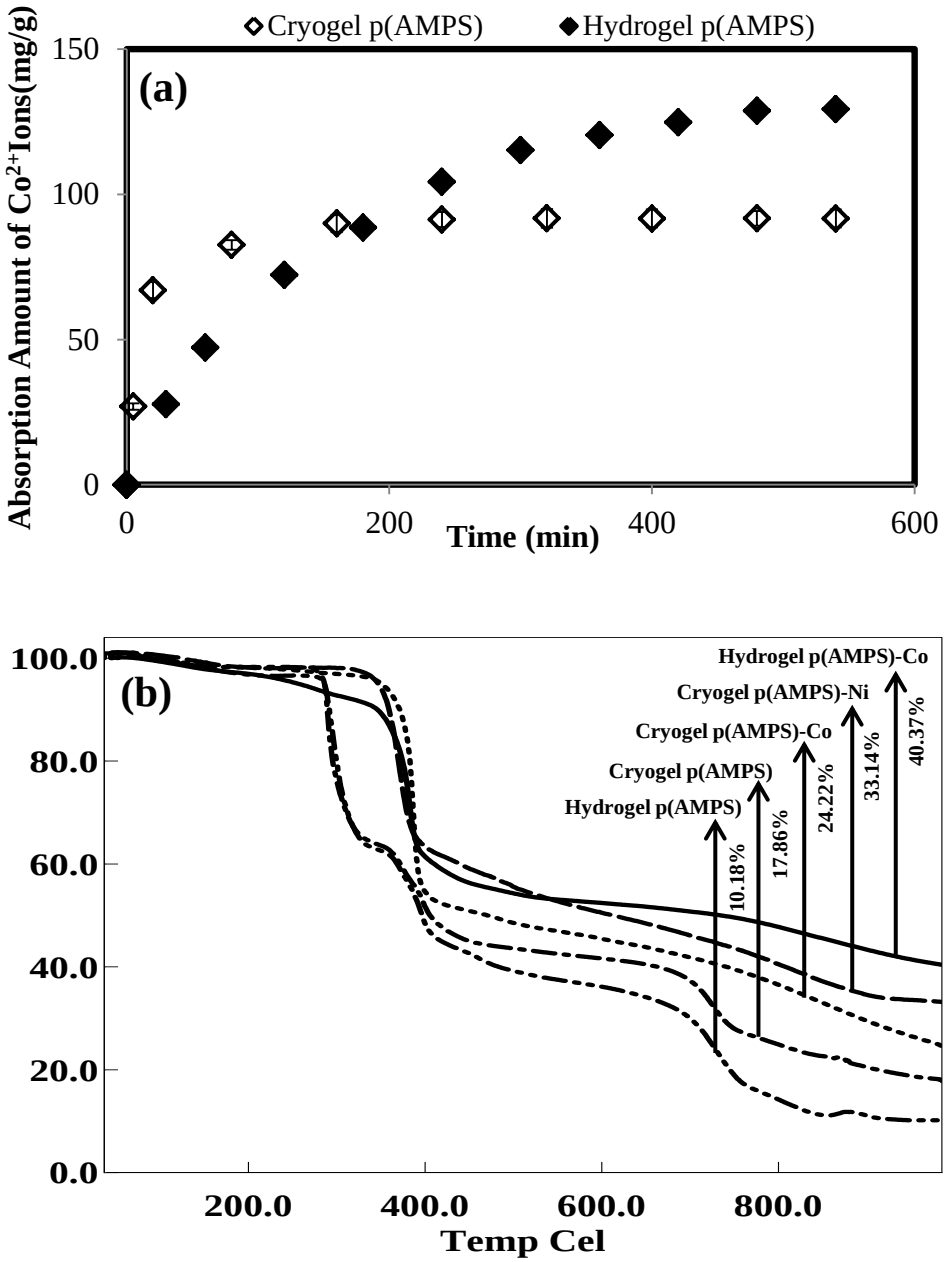

Figure 4. (a) Metal ion absorption capacities of p(AMPS) hydrogel and cryogel, and **(b)** TGA thermogram of p(AMPS) hydrogel, cryogel and their metal nanoparticle-containing composites.

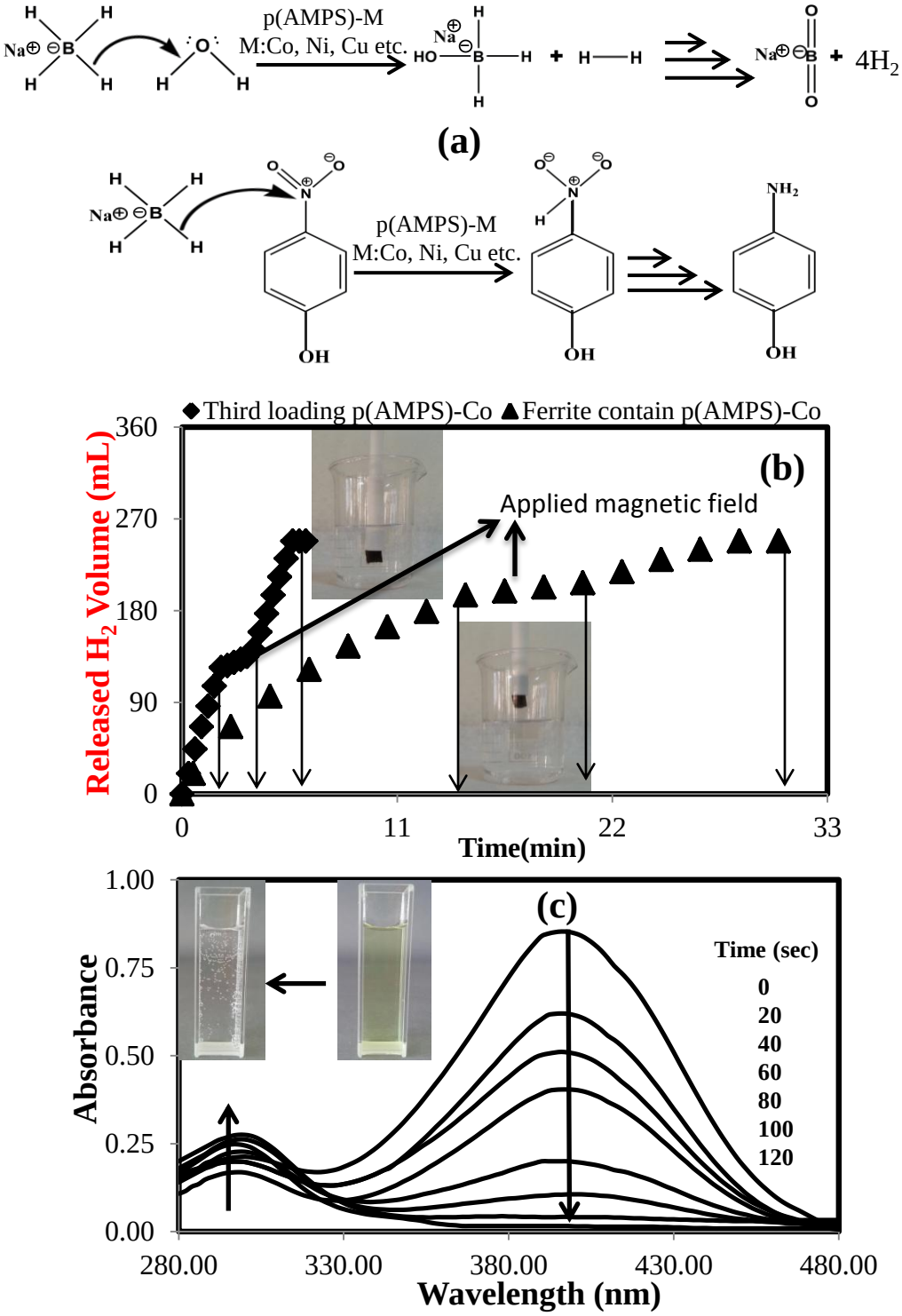

Figure 5. (a) Reaction mechanisms of H_2 generation from hydrolysis of $NaBH_4$, and reduction of 4-NP. **(b)** H_2 generation from hydrolysis of $NaBH_4$ via ferrite-containing 0.1 g p(AMPS)-Co metal nanoparticles (8.71 mg nanoparticles) and magnetic three times Co(II) loaded-reduced 0.1 g p(AMPS)-Co (19.54 mg/g nanoparticles) catalyst system under externally applied magnetic field. [Reaction conditions: 50 mL 50 mM $NaBH_4$, 5 wt% NaOH, 30 °C, 1000 rpm mixing rate.] **(c)** UV–Vis spectra of 4-NP reduction to 4-AP by using 0.1 g p(AMPS)-Co cryogel composite catalyst systems (8.62 mg Co nanoparticles) [Reaction conditions: 50 mL 0.01 M 4-NP, 0.28 M $NaBH_4$, 30 ºC, 1000 rpm mixing rate].

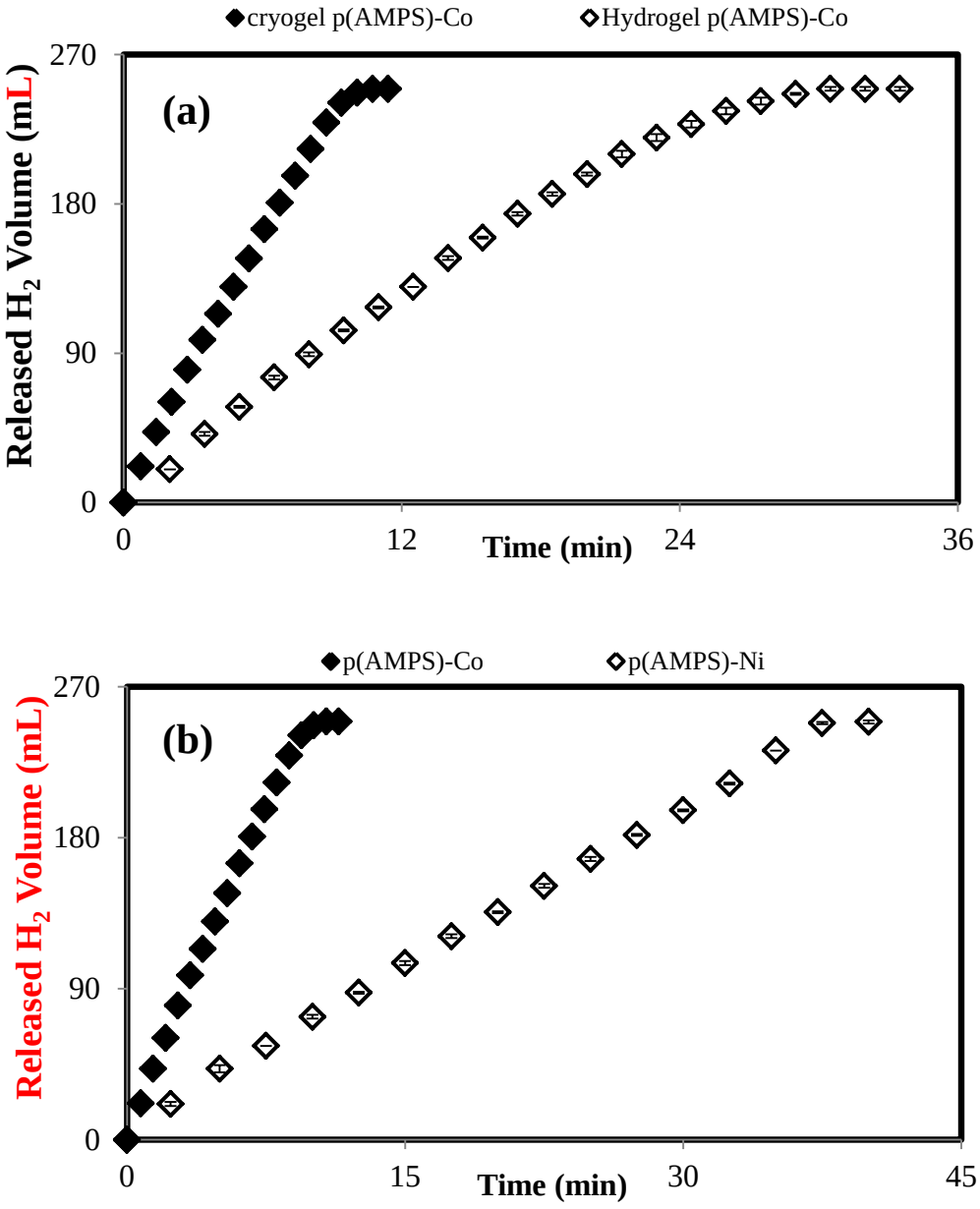

Figure 6. **(a)** H_2 generation from hydrolysis of 50 mL 50 mM $NaBH_4$ via 8.62 mg Co nanoparticle-containing 0.1 g cryogel p(AMPS)-Co composite, and 0.069 g hydrogel p(AMPS)-Co composites. [Reaction conditions: 50 mL 50 mM $NaBH_4$, 5 wt% NaOH, 30 °C, 1000 rpm.]
(b) H_2 generation from hydrolysis of $NaBH_4$ via 0.1 g cryogel p(AMPS)-Co (8.62 mg Co nanoparticles) and 0.1 g p(AMPS)-Ni composites (8.94 mg Ni nanoparticles). [Reaction conditions: 50 mL 50 mM $NaBH_4$, 5 wt% NaOH, 30 °C, 1000 rpm.]

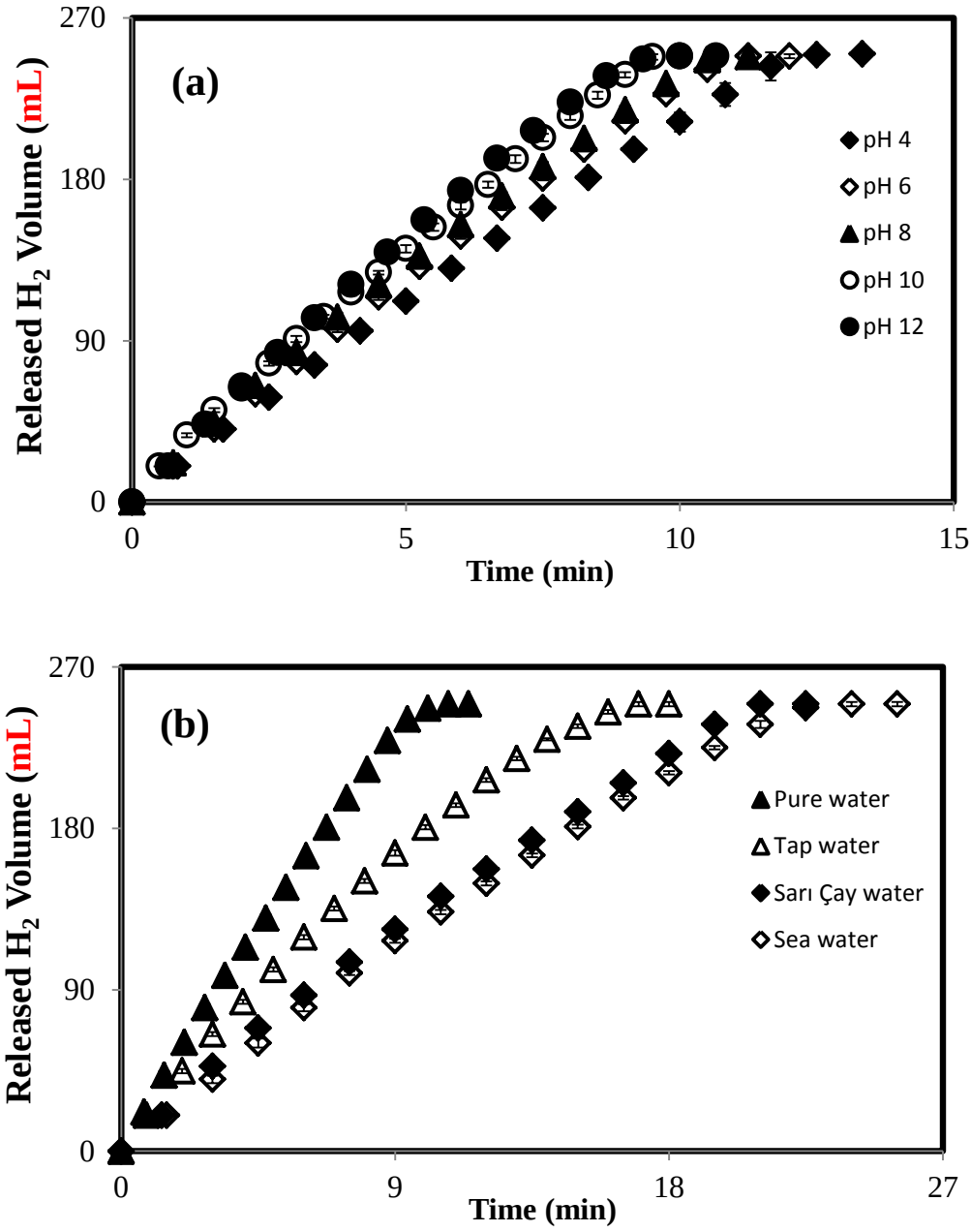

Figure 7. (a) The effect of pH and **(b)** the effect of water type on H_2 generation reaction from hydrolysis of sodium borohydride via 0.1 g cryogel p(AMPS)-Co (8.62 mg nanoparticles). [Reaction conditions: 50 mL 50 mM $NaBH_4$, 5 wt% NaOH, 30 °C, 1000 rpm].

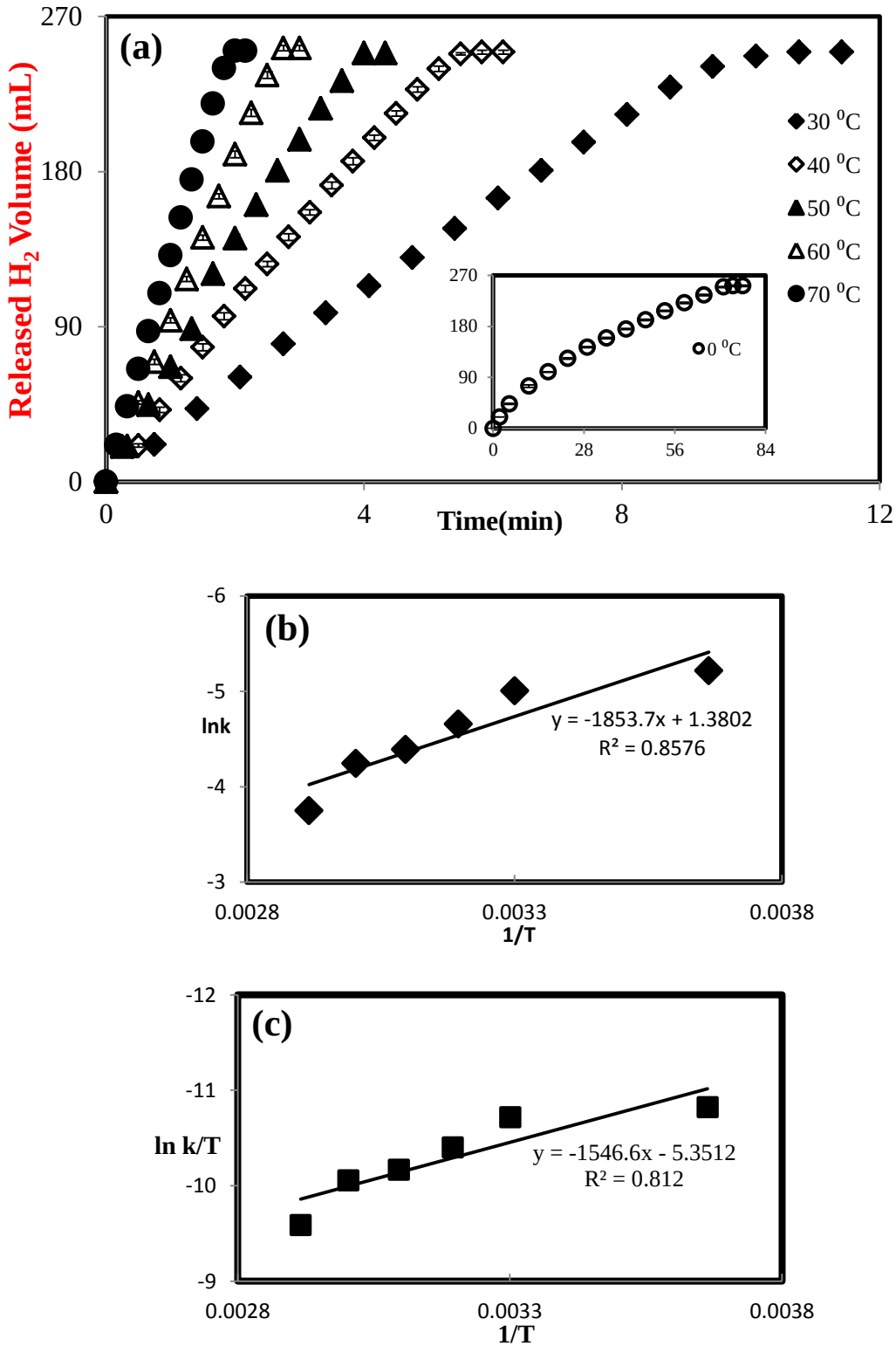

Figure 8. (a) The effect of temperature on the hydrolysis of $NaBH_4$, **(b)**, ln k versus 1/T (Arrhenius eq.), and **(c)**, ln (k/T) versus 1/T (Eyring eq.) [Reaction Conditions: 50 mL 50 mM $NaBH_4$, 5 wt% NaOH, 1000 rpm, 8.62 mg Co nanoparticles in 0.1 g cryogel p(AMPS)-Co composite].

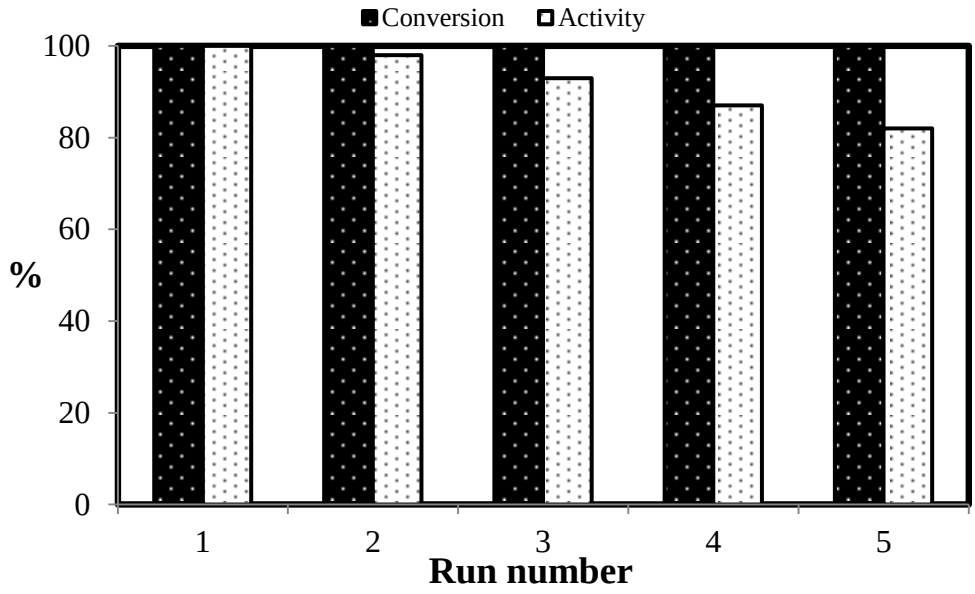

Figure 9. The activity and the conversion ability of the cryogel p(AMPS)-Co composite for repetitive $NaBH_4$ hydrolysis [Reaction conditions: 50 mL 50 Mm $NaBH_4$, 5 wt% NaOH, 30 °C, 1000 rpm, 8.62 mg Co nanoparticle in 0.1 g cryogel].

Cite this: DOI: 10.1039/c0xx00000x

www.rsc.org/xxxxxx

ARTICLE TYPE

Energy and Environmental Usage of Super Porous Poly(2-acrylamido-2-methyl-1-propan sulfonic acid) Cryogel Support

***Nurettin Sahiner[a,b] and Fahriye Seven[b]**

Received (in XXX, XXX) Xth XXXXXXXXX 20XX, Accepted Xth XXXXXXXXX 20XX

DOI: 10.1039/b000000x

Superporous and nonporous poly(2-acrylamido-2-methyl-1-propansulfonic acid) p(AMPS) cryogels and hydrogels were prepared under freezing conditions (-18 °C) and at room temperature (25 °C), respectively. P(AMPS) cryogels showed super fast swelling equilibrium values, 3600 fold faster than conventional hydrogels. The p(AMPS) cryogels were further employed as highly effective support for in situ metal nanoparticle preparation within superporous networks by loading Co (II) and Ni(II) ions into the cryogel network from aqueous environments and reducing with $NaBH_4$. The Co metal nanoparticle-containing cryogel composites demonstrated superior catalytic performances in comparison to nonporous p(AMPS) hydrogel composites for energy and environmental applications e.g., hydrogen production from hydrolysis of sodium borohydride, and reduction of 4-Nitrophenol to 4-Aminophenol. The energy applications of cryogel-based p(AMPS)-Co metal composites, especially, were investigated in detail. The effect of various parameters on the rate of the hydrogen generation reaction, such as porosity, metal types, pH, the types of reaction water, temperature and reuse of catalyst, were examined for p(AMPS)-Co cryogel composite materials. With the p(AMPS)-Co cryogel composite a very high hydrogen generation rate of 14501 (mL H_2) $(min)^{-1}$ (g of Co)$^{-1}$ was attained. This value is one of the best recorded values in comparison to other similar catalysts reported in the literature. P(AMPS)-Co composite cryogels were repeatedly used without significant loss of catalytic activity (82%) even after five repetitive uses for the catalytic hydrolysis reactions with $NaBH_4$. Additionally, a very low activation energy for p(AMPS)-Co cryogel composite systems was attained; Ea=15.40±0.3 kJmol^{-1}.

Kew words: Cryogels, hydrogels, catalyst, sodium borohydride, hydrogen production, environmental application.

1. Introduction

In recent years, innovative research has been realized with regard to energy and environmental concerns [1,2]. Energy is essential to maintain all activities in daily life. However, the production, transportation and the use of energy, which is obtained principally from fossil fuels, forms the root of major adverse effects on the environment and on health. Therefore, the generation of renewable, clean and inexhaustible energy has crucial significance [3,4]. Many researchers have focused on hydrogen energy as renewable, clean, safe, cheap and even easily generated from hydrolysis of various storage materials such as chemical hydrides [5,6]. In addition to drawbacks in energy production, the major concern for the environment and human health are the existence of hazardous organic toxic chemicals. Amongst organic pollutants halogenated organic compounds, and their derivative nitrophenols (4-NP), are a major concern because of their high toxicity, carcinogenic nature, and low biodegradability, which accumulate in wastewater and cause many problems as they are used in many industries such as the production of anilines, paper, explosives, pharmaceuticals, dyes and others [7,8]. Due to the favorable properties such as selective strong reducing capability, hydrogen generator and storage material, and usefulness in manufacturing pharmaceuticals, and fine chemicals, $NaBH_4$ is a preferred material attracting great attention over the past decade and one of the mostly frequently used materials for various applications, as stated earlier [9-11]. $NaBH_4$ can be used for both hydrogen generation from the hydrolysis reaction in the presence of a catalyst, and in the reduction of toxic nitrophenols and its derivatives to environmentally friendly amino phenols [12,13]. In use of metal nanoparticles as catalysts, aggregation problems, and stabilization of metal nanoparticles (generally ~5-100 nm) to prevent early oxidation and poisoning, are the most cumbersome problems and can be overcomed by employing nanotechnology and polymer science [14,15]. Recently, we have reported smart hydrogel usage as template for metal nanoparticle preparation taking advantages of hydrophilic 3-D networks that have different numbers of functionalities including –OH, –COOH, $–NH_2$, $–CONH_2$, and $–SO_3H$ with high metal binding ability in aqueous media without dissolving. They provide a range of environmentally responsive behavior, such as bending, degrading, swelling, shrinking, and color changing against environmental factors such as pH, solvent, temperature, electric field, magnetic field, etc. [16-18]. Despite these advantages of common hydrogels, the diffusion of solvents, metal ions or any reactant into the hydrogel network remains the foremost tiresome and time consuming problems for in situ nanoparticle preparation within the hydrogel network or usage as

reactants in the catalytic applications. To improve their responsive properties, nano, micro and macro pores can be generated within hydrogel networks by various techniques. One alternative solution is to use hydrogel networks with macro or super pores (on the order of a few tens of micrometers) that can be generated within hydrogels by preparing them in cryogenic conditions, named as cryogels. Recently much progress in the cryogelation method by preparing hydrogels under cryogenic conditions has been made [19-22]. The cryogelation method includes the use of a large amount of pure water, nearly 90-95 wt% of the initial solution. The polymerization and crosslinking reaction can be carried out around frozen water molecules (ice-crystals) under freezing conditions. During the polymerization reaction, most of the water molecules are converted to ice crystals, whereas bound water and other solutes in the reaction medium, such as initiator, crosslinking agent, catalyst and monomer molecules, accumulate in a non-frozen liquid microphase [23-25]. Cryogenic network formation progresses via polymerization of the non-frozen liquid microphase around the ice-crystals that act as porogen. Upon thawing the ice-crystals within gel matrices, a superporous cryogel is formed that has large pores with variable size and geometry depending on the shape of ice-crystals [26, 27]. Furthermore, natural characteristics of cryogels, such as super pore size, pore wall thickness, elasticity, and mechanic strength, can be tuneable by adjusting the preparation conditions, and the composition of solutions, such as the amount of water or organic co-solvents, cooling rate, temperature gradient, solute concentrations, precursor composition, etc. Interconnected macropores within the three-dimensional cryogenic networks enable retention and release of water or any solvent which is absorbed within large pores with diffusion pathway via reversible squeeze-relaxation cycles under definite pressure [28-31]. Due to their discernible properties, most notably fast responsiveness, structural flexibility, high mechanical resistance, large pores, and fast diffusion pathways, cryogels can respond to external stimuli such as pH, solvent, and ionic strength etc much faster than conventional hydrogels [32, 33]. Moreover, these properties of cryogels make them ideal fast metal ion binding material, and catalyst support for in situ metal nanoparticle preparation [16-18]. The cryogel containing metal composites can be used as catalyst in H_2 generation for energy applications, and reduction of nitro compound for environmental applications.

Therefore, we report the use of p(AMPS) cryogels and hydrogels prepared by free radical polymerization technique at freezing and room temperatures, and used for in situ metal nanoparticle preparation by loading Co and Ni ions from their aqueous solutions and reduction. Finally, we also demonstrated the use of p(AMPS)-M (M: Co, Ni) cryogel composites in H_2 generation via $NaBH_4$, and in an environmental application for reduction of 4-NP to 4-AP. Various parameters affecting the H_2 generation performance were evaluated and compared with the literature.

2. Materials and Methods

2.1. Materials

The monomer, 2-acrylamido-2-methyl-1-propanesulfonic acid (AMPS, 50 wt%, Sigma-Aldrich), the crosslinker, N,N□-methylenebisacrylamide (MBA, 99%, Across), the initiators, ammonium persulfate (APS, 99%, Sigma-Aldrich) or potassium persulfate (KPS, 99%, Sigma-Aldrich), and the accelerator, N,N,N',N'-tetramethylethylene diamine (TEMED, 98%, Across) were used in hydrogel and cryogel preparation as received. Cobalt(II) chloride hexahydrate ($CoCl_2.6H_2O$, 99%, Sigma-Aldrich) and nickel(II) chloride hexahydrate ($NiCl_2.6H_2O$, 98%, Sigma-Aldrich) were used as metal ion sources in nanoparticle preparation. Sodium borohydride ($NaBH_4$, 98%, Merck) was used as reducing agent and H_2 source in the hydrolysis reaction. 4-Nitrophenol (4-NP, 99%, Merck) was used as organic compound in the catalytic reduction reaction. Sodium hydroxide (NaOH, 97%, Sigma-Aldrich), and hydrochloric acid (HCl, 37%, Sigma-Aldrich) were used for the preparation of acidic and basic solutions. Tap water, water from Sarı Çay creek, and sea water were used as reaction media in the same hydrogen generation reactions. The distilled (DI) water of 18.3 MΩ.cm was used for experimental studies.

2.2. Synthesis of P(AMPS) Hydrogels and Cryogels

Synthesis of p(AMPS) hydrogel was carried out via free radical polymerization technique. Briefly, 5 mL AMPS, 0.002 g MBA (0.1% mole ratio of monomer) and 5μL TEMED were mixed to obtain a homogenous solution, and 1 mL of APS initiator solution (1% mole ratio of monomer) was added by mixing, and the obtained hydrogel precursor was placed in plastic straws of about 0.4 mm diameter. The reaction was completed within 15 min and the obtained cylindrical hydrogels were cut 2-3 mm in length, and washed with DI water for 12 h by placing in excess amounts of water and replacing water every three hours.

The preparation of p(AMPS) cryogel was performed via cryopolymerization technique. An ice bath was used to cool AMPS precursors before cryopolymerization. Firstly, 0.78 mL AMPS aqueous solution (50 wt%) was added into 6.22 mL DI water in order to complete the total amount of monomer ratio to 6 w/v% within total solution volume of 8 mL solution. Then, 0.0354 g MBA (10% mole ratio of monomer), and 50 μL TEMED were added into the monomer solution and mixed by using a vortex mixer. Separately, 0.0054 g of KPS (1% mole ratio of monomer) was dissolved in 1 mL DI water, and cooled under constant mixing in an ice-bath for 5 min. Finally, this redox initiator solution was added into the cooled monomer mix, and then this mix was placed in plastic straws (about 8 mm in diameter). The cryogelation was achieved in a deep freezer at -18 ºC for 24 h via free-radical crosslinking polymerization. Finally, the obtained cryogels were thawed at room temperature, and cut into smaller dimensions of 2-3 mm. The acquired cryogels were cleaned by washing with plenty of DI water to remove unreacted species such as monomer, polymer, crosslinker and initiator from the cryogenic matrices. The obtained cryogels were dried in an oven at 45 °C for further experimental studies.

2.3. Synthesis of Metal Nanoparticles within Conventional Hydrogel and Superporous P(AMPS) Cryogel Matrices

The preparation of metal nanoparticles inside the network structure was carried out by metal loading from aqueous solutions and in situ reduction. Briefly, 100 mg of dried hydrogel and cryogel samples were placed into 100 mL 500 ppm M (II) (M=Co or Ni) solutions under the constant mixing rate of 500 rpm, at room temperature, for 24 h. Then, to remove unattached metal ions from polymeric networks, metal ion-loaded polymeric networks were washed with distilled water for 30 min. After washing, the metal ion-loaded hydrogels and cryogels were placed into 50 mL 0.2 M $NaBH_4$ solution for 3 h under 500 rpm stirring rate at room temperature for reduction of metal ions in situ within the polymeric networks to their corresponding metal nanoparticles. Finally, hydrogel or cryogel-M composites were washed with DI water again, and used for catalytic applications.

3. Results and Discussion

3.1. Characterization of Nonporous, Superporous Polymeric Networks and Their Metal-Containing Composites

The swelling characteristics, pore sizes and pore structures of conventional hydrogel and novel cryogel networks were

determined through swelling experiments, optical microscope (Olympus bX53) and scanning electron microscope (SEM, JEOL 2010) analysis. The metal ion absorption capacity and the metal nanoparticle contents of the hydrogel and macroporous cryogel were determined with atomic absorption spectroscopy (AAS, Thermo ICA 3500 AA SPECTRO) measurements. The size of metal particles inside the bulk cryogel matrices was determined via transmission electron microscopy (TEM, JEOL 2010) analysis. Finally, the thermal behaviour of hydrogels, cryogels and their various metal composites were investigated by thermogravimetric analysis (TGA/DTA-SII 6300).

To visualize the mechanism of cryopolymerization, the representation of the cryopolymerization reaction of the non-frozen liquid microphase occurring around growing ice-crystals is illustrated in Figure 1(a). Firstly, initiator activated by catalyst and generated radicals react with the monomer and crosslinker to produce branched oligomers and macromers etc., and upon the progress of polymerization and crosslinking reaction around ice-crystals as seen in representation frozen cryogel network is obtained. Upon the complation of polymerization and the crosslinking reaction, and after thawing, macrometer size of pores in the places of ice-crystals within the 3-D polymeric matrices are obtained as can be seen in the representation of the figure.

As swelling behaviour is one of the most important characteristics of hydrogels, the swelling behaviour of p(AMPS) hydrogels and cryogels was investigated. The swelling studies of hydrogel and cryogels were carried out by means of mass increase by placing the dried and weighed polymeric networks within 100 mL distilled water, removing them at certain time intervals and determining their mass increase with time. The maximum percent swelling of hydrogel and cryogels (Smax %) were calculated as about 28000% and 500% according to equations 1 and 2. So, the high swelling degree of 0.1 mole % crosslinked p(AMPS) hydrogels implies that that it has higher amounts of water (~56 fold) than those of 10% crosslinked p(AMPS) cryogels.

$$\%S = [(m_{\text{wet hydrogel}}-m_{\text{dry hydrogel}})/m_{\text{dry hydrogel}}]x100 \quad (1)$$

$$\%S= [(m_{\text{squeezed cryogel}}-m_{\text{dry cryogel}})/m_{\text{dry cryogel}}]x100 \quad (2)$$

As illustrated in Figure 1(b) and (c), the time to reach S_{max}% for hydrogel and cryogels are quite different from each other with hydrogels reaching their S_{max}% at about 8 h, whereas cryogels completed S_{max}% within 10 sec. It is obvious that the swelling time for superporous cryogels is almost 3600 times shorter than its corresponding conventional hydrogel, even though it has 100 fold more crosslinks with lower swelling ratio. In fact, this behaviour is due to differences in their preparation methods. Keeping in mind that cryogels have a high degree of crosslinker with very large interconnected porous structure and low specific surface area compared to their counterpart hydrogels, they therefore swell quickly, within seconds, with small amount of water uptake in comparison to normal hydrogels [34,35]. The fast swelling property of cryogels provides many advantages. For example, the main advantages of the higher swelling rates, and faster swellings of cryogels provide fast process times in cleaning of cryogels, and loading of cryogels with different species such as metal ions and their reduction to corresponding metal nanoparticles, and eventually provide faster catalytic performances in their catalytic applications.

Furthermore, % porosity of cryogels was roughly calculated as 78.60% according to the following equation:

$$\%\ \text{Porosity} = [(m_{\text{wet cryogel}}-m_{\text{squeezed cryogel}})/m_{\text{wet cryogel}}]x100 \quad (3)$$

The interconnected and highly open structures of p(AMPS) cryogels were examined through SEM analysis, and the optical microscope images as illustrated in Figure 2(a) thru (f). The pore structures of dried p(AMPS) cryogel samples were obtained as a thin film using a freeze-dryer under a vacuum. As can be seen in Figure 2(a)-(f), the pore size of the cryogels was more than 50 µm. Highly interconnected and open pores of cryogels provide faster contact time with the metal nanoparticles embedded within them with reactants in reaction medium. It is obvious that this highly porous network and fast responsive nature of cryogels make them indispensable materials in design of advanced template materials e.g., for metal nanoparticle preparation and use as catalyst systems for catalytic applications. Here, we prepared Co and Ni metal nanoparticles as catalyst systems by using $NaBH_4$ as reducing agent within p(AMPS) cryogels via in situ reduction method. For that purpose, Co(II) or Ni(II) metal ion-loaded 0.1 g p(AMPS) cryogels were treated with 50 mL 0.2 M $NaBH_4$ solution at 500 rpm mixing rate for 3 h. As clearly demonstrated in Figure 3(a), Co(II) ions inside cryogel matrices were converted to Co metal nanoparticles by $NaBH_4$ treatment. Furthermore, the TEM images of p(AMPS)-Co composites show that size of Co metal particles are nanoscale, ranging from about few tens of nm to about 50 nm as seen in Figure 3(b). The TEM images were obtained by grinding samples of p(AMPS)-Co composite suspension in acetone and a few drops these composite were placed on carbon coated Cu TEM grids. The TEM images were then acquired under the electron beam, accelerated by the applied 200 kV in vacuum. As demontrated in TEM images, Co particles are almost homogeneously distributed throughout the p(AMPS) cryogel matrices.

Fast responsive behavior of porous p(AMPS) cryogels and corresponding hydrogels were compared in terms of Co(II) ion absorption times and amount as illustrated in Figure 4(a). About 1.0 g of p(AMPS) cryogel and hydrogels were immersed within 500 mL 500 ppm $CoCl_2.6H_2O$ solution at 500 rpm mixing rate. It was found that 91.70 mg Co(II) ions were absorbed by cryogels at the end of 4 h, whereas 129.35 mg Co(II) ions were absorbed by hydrogels at the end of 8 h. Although the Co(II) ion absorption time of cryogels is about two fold shorter than the hydrogel, the Co(II) ion absorption capacity is much less than the hydrogel. This is generally the case for cryogels as because of the low specific surface area of cryogel than hydrogels of p(AMPS). The only downside of cryogels is their lower specific surface area as was reported in the literature [34, 35]. In addition to the comparison of their metal ion absorption capacities, the metal nanoparticle contents were also determined via an acid dissolution method in which metal nanoparticle-containing cryogels and hydrogels were treated with concentrated HCl. Thus, 0.1 g of p(AMPS)-M (M:Co or Ni) composites were treated with 50 mL 5M HCl solution for 12 h three times repeatedly, and the elution solution was diluted at the ratio of 1/150 with pure water. The amount of metal ions within each polymeric matrix was measured by AAS. The amount of Co nanoparticles within one gram cryo-p(AMPS) was found to be 86.27 mg/g, whereas the amount of Co metal nanoparticles inside one gram of hydrogel-p(AMPS) was 124.88 mg/g. As can be seen these values are consistent with their absorbed amounts. The amounts of metal contents of cryogels and hydrogels are given in Table 1. Additionally, the metal content of each polymeric matrix was also confirmed via thermogravimetric analysis as seen in Figure 4 (a) and Table 1. Thermal behavior of p(AMPS) cryogels, hydrogels and their metal particle-containing composites were determined via thermogravimetric analyzer by heating about 2 mg of dried samples from 50 to 1000 ºC with 10 ºC/min heating rate under nitrogen flow of 100 mL/min. As can be seen, the thermal behavior of p(AMPS) cryogels and hydrogels seem very similar whereas their metal nanoparticle-containing composites are

different, depending on the metal types and their amounts. It can be inferred that p(AMPS) cryogels and hydrogels start to degrade very sharply at about 300 °C, whereas the onset of sharp degradation for their metal nanoparticle-containing composites is about 350 °C. The p(AMPS) cryogels and hydrogels and their composites have different degradation temperatures as shown in TGA thermograms and this continued up to 1000 °C as illustrated in Figure 4(b). The weight losses of p(AMPS) cryogels and their Co nanoparticle-containing composites were found as 22.58 and 17.65 wt%, whereas the weight losses of p(AMPS) hydrogels and their Co composites were 44.45 and 10.18% at 985 °C. Consequently, due to the high crosslinking degree of cryogels, they have shown higher thermal stability than conventional hydrogels. On the other hand, due to their low metal nanoparticle contents, their composites have shown less thermal stability than metal composites of hydrogels. The thermal resistances of other metal composites are given in Table 1, and it shows that the metal nanoparticle-embedded p(AMPS) networks, whether hydrogel or cryogel, are thermally more stable and have less sharp degradation temperature ranges than their bare hydrogel or cryogels counterparts. Therefore, it can be concluded that from TGA analysis, p(AMPS) cryogel metal composites can be safely used in the temperature range of room temperatures to up to 200 ^{o}C without any significant weight loss. The higher thermal stability of the cryogels could be due to high amount of used crosslinker for cryogels than hydrogels as the crosslinking degree of cryogels approximately hundred fold higher than those of hydrogels.

3.2. Energy and Environmental Applications of p(AMPS)-Co Metal Composites

To demonstrate the potential use of p(AMPS) hydrogel and cryogel in energy and environmental applications, H_2 generation and reduction of 4-NP were carried out by using $NaBH_4$ as hydrogen source, and as reducing agent by using p(AMPS)-M based materials as catalyst. The reaction mechanisms of both catalytic reactions are shown in Figure 5(a). Interestingly, magnetic ferrites can also be used for $NaBH_4$ hydrolysis for H_2 generation, as well as Co and Ni nanoparticles. Here, two types of magnetic metal nano particle ferrite and Co containing metal nanoparticles prepared within p(AMPS) cryogels were used in H_2 production from hydrolysis of NaBH4. As illustrated in Figure 5(b), the inherently magnetic field responsive behavior of a catalyst offers control over the reaction system by an externally applied magnetic field. The preparation of ferrite metal nano particles was done according to the literature [16], briefly, 0.1 g p(AMPS) cryogels were immersed within a metal ion solution containing 1:2 mole ratio of Fe (II) (0.05 M):Fe (III) (0.1 M) mixture in 100 mL aqueous solution for 12 h. Then, these iron ion-loaded cryogels were washed for 1 h to remove unbound metal ions from the cryogel matrices, and then placed in 100 mL 0.5 M sodium hydroxide solution for 5 h to convert iron ions into ferrite magnetic particles. Additionally, magnetic p(AMPS) cryogels were also prepared with Co (II) ions after three loading and reduction cycles as mentioned in section 2.3. After the first loading and reduction of Co(II) ions into p(AMPS) cryogels, the prepared p(AMPS)-Co composites were placed again in 500 mL 500 ppm Co(II) ion solution for 5 h, and then reduced to metal nanoparticles with 50 mL 50 mM $NaBH_4$ solution for 3 h treatment, and the same procedure was repeated three times to increase the Co metal nanoparticle content of p(AMPS) cryogel with magnetic field responsive behavior. The use of magnetic metal nanoparticles is very important to control the reaction e.g., the catalyst systems can be removed from the reaction mixture and placed back into the reaction medium to control the catalytic reactions. As illustrated in Figure 5(b), H_2 generation from hydrolysis of $NaBH_4$ by using 0.1 g ferrite-containing p(AMPS)-Co (containing 8.71 mg Co nanoparticles) were stopped at 12.5 min by removing the catalyst system from the reaction medium, and continued at 22.5 min by placing back into the reaction medium. The reaction conditions throughout this investigation are 50 mL 50 mM $NaBH_4$, 5 wt% NaOH, 30 °C, 1000 rpm mixing rate. The same H_2 production control was done by using 3rd time Co(II) loaded and reduced p(AMPS)-Co composite cryogel catalyst system (containing 19.54 mg Co nanoparticles) at 2 and 4 min under the same conditions. The hydrolysis reaction was completed within 30 min with ferrite-containing p(AMPS)-Co metal composite catalyst system whereas the hydrolysis reaction was completed in only 6 min with three times-loaded p(AMPS)-Co cryogel composite catalyst system. Therefore, the inherently magnetic field responsive p(AMPS)-Co cryogel catalyst system provides great advantage in controllable fast catalysis for energy applications. Moreover, the environmental application of p(AMPS) cryogel catalyst system was demonstrated by using 0.1 g p(AMPS)-Co metal composite for reduction of 4-NP to 4-AP as illustrated in Figure 5(c). The reduction of 4-NP was carried out using 50 mL 0.01 M 4-NP by using first time Co(II) loaded and reduced p(AMPS)-Co cryogel composite catalyst system (containing 8.62 mg nanoparticles) in the presence of 50 mL 0.28 M $NaBH_4$ at 30 °C and 1000 rpm mixing rate. The reduction of 4-NP was completed within 120 seconds by cryogel-based p(AMPS)-Co metal composites. This time is relatively fast in comparison to the reported values in the literature [13,16, 36, 40-44], suggesting that cryogel-based catalyst composite systems have great advantages for faster catalytic performances. When considering these results and comparing with papers reported in the literature, highly porous, large and open interconnected structures of cryogels provide great benefit in iterms of fast reaction kinetics [16, 40-44]. Therefore, the choice of superporous cryogels as catalyst support, and reaction media in catalytic application is pertinent.

3.3. The Effect of Porosity and Metal Types on $NaBH_4$ Hydrolysis

To determine the effect of porosity, H_2 production rates of conventional hydrogel and superporous cryogel p(AMPS)-Co composites were compared under equal reaction conditions; for example, 0.1 g cryogel p(AMPS)-Co composites (containing 8.62 mg nanoparticles) and 0.069 g hydrogel p(AMPS)-Co composites (containing 8.62 mg nanoparticles) were used for the hydrolysis of 50 mL 50 mM $NaBH_4$, 5 wt% NaOH content, at 30 °C, 1000 rpm mixing rate. The same amount of hydrogen was produced, nearly 250 mL, from the hydrolysis reactions and it was completed within about 10 min by cryogel p(AMPS)-Co composites and the same reaction was completed by the end of 30 min via hydrogel p(AMPS)-Co composites as illustrated in Figure 6(a). The H2 production rate of cryogel p(AMPS)-Co composites is three times faster than conventional hydrogel-supported metal composites. At the same time, as shown in Table 1, the Hydrogen Generation Rate (HGR), and Total Turnover Frequency (TOF) value of hydrogel p(AMPS)-Co composites were calculated as about 950 (mL H_2) $(min)^{-1}$ (g of metal)$^{-1}$ and 2.24 (mol H_2) (mol catalyst min)$^{-1}$, whereas the HGR and TOF values of cryogel p(AMPS)-Co composites were calculated as 2697 (mL H_2) $(min)^{-1}$ (g of M)$^{-1}$ and 6.37 (mol H_2) (mol catalyst min)$^{-1}$, respectively. These values are 2.839 times and 2.844 times higher for the cryogel catalyst system, confirming the great benefit of porosity. Porosity of cryogels provides easy and fast diffusion of reactants and products in an out of cryogel matrices and other species enabling faster kinetics with embedded metal nanoparticles inside pores. This phenomenon is main reason and it is most prominent distinct features of catalytic activity of porous catalyst or cryogels so to say.

The different metal nanoparticles were prepared within cryogel matrices, and their catalytic performances were compared in the hydrolysis of $NaBH_4$ under the same reaction conditions as shown in Figure 6(b). As can be seen, H_2 generation from the hydrolysis of $NaBH_4$ was completed in about 10 min by using 0.1 g p(AMPS)-Co composites (containing 8.62 mg nanoparticles) whereas the same reaction was completed in about 40 min by p(AMPS)-Ni composites (containing 8.94 mg nanoparticles) under the same reaction conditions. The HGR of cryogel p(AMPS)-Co and p(AMPS)-Ni composites were calculated to be 2700 and 700 (mL H_2) $(min)^{-1}$ (g of metal)-1 as given in Table 1. It is obvious that HGR of Co nanoparticle-containing p(AMPS) cryogels was nearly fourfold faster than Ni nanoparticle-containing p(AMPS) cryogels, as expected since Co nanoparticle catalytic performance is better than Ni nanoparticles in accordance with literature [16, 17, 37-44].

3.4. The effect of pH of the Reaction Medium and Type of Water on $NaBH_4$ Hydrolysis

To determine the effect of pH of the medium on the hydrolysis reaction of $NaBH_4$ employing 0.1 g p(AMPS)-Co metal composite (containing 8.62 mg nanoparticles) under the same reaction conditions, five different pH values were tested i.e., 4, 6, 8, 10 and 12 as shown in Figure 7(a). To adjust the pH of the reaction medium, 1M HCl or 1M NaOH were added into the hydrolysis medium and the obtained solutions with different pHs were used for the hydrolysis reaction of $NaBH_4$. Although the amount of produced H_2 gas was not affected by the change of medium pH, they all produced about 250 mL H_2, the HGR of p(AMPS)-Co composites were affected as can be seen from the slope of Figure 7(a). As can clearly be seen, as the pH of the $NaBH_4$ solution increased, the HGR also increased. The fastest hydrolysis reaction occurred at pH 12, and it reduced with decreasing pH values. In other words, the H_2 generation reaction of $NaBH_4$ was completed in about 10 min at pH 12, whereas the same reaction was completed in about 13 min at pH 4. Furthermore, HGR and TOF value of p(AMPS)-Co composite systems were calculated for different pHs and it was found that they both increased as the pH increased as given in Table 2. As the $NABH_4$ hydrolysis is generally performed in basic media these results comply with the literature [16, 40-44].

The hydrolysis reaction of $NaBH_4$ was also performed in four different types of water; pure water, tap water, Sarı Çay (local creek) water, and seawater, via 0.1 g p(AMPS)-Co composites (containing 8.62 mg nanoparticles) at the prescribed reaction conditions. As seen in Figure 7(b), the HGR of p(AMPS)-Co composites were strongly affected by the type of reaction water source. The fastest hydrolysis reaction, or highest HGR, was obtained in pure water whereas the slowest hydrolysis reaction, or the lowest HGR, was obtained in seawater. As can be seen from the figure, the H_2 generation reaction of $NaBH_4$ was completed within about 10 min in pure water, while the H_2 generation reaction of $NaBH_4$ was completed in about 25 min with seawater. The calculated HGR and TOF values were about 1288.99±1.3 (mL H_2) $(min)^{-1}$ (g of M)$^{-1}$ and 3.03±0.5 (mol H_2) (mol catalyst $min)^{-1}$ for seawater in comparison to 2697.91±1 (mL H_2) $(min)^{-1}$ (g of M)$^{-1}$ and 6.37±0.4 (mol H_2) (mol catalyst $min)^{-1}$ for DI water as illustrated in Table 2. As known, the saltiness of sea water is higher than other type waters as compared with Sarı çay water a creek water, tap water and DI water that prevents to attain higher TOF, and HGR values. In brief, due the presence of different salts and some other impurities within seawater, creek waters, tap waters, the reduction in HGR and TOF valuables are plausible.

3.5. The Effect of Temperature on $NaBH_4$ Hydrolysis

The effect of temperature on the hydrolysis of $NaBH_4$ was scrutinized by using 0.1 g p(AMPS)-Co composites at different temperatures between 30 ºC and 70 ºC with 10 ºC increments under the same reaction conditions: 50 mL 50 mM $NaBH_4$ (containing 5 wt% NaOH),1000 rpm mixing rate, using 0.1 g p(AMPS)-Co (containing 8,62 mg/g Co). In addition, the hydrolysis reaction of $NaBH_4$ was also investigated under relatively colder conditions e.g., 0 ºC. This process was carried out in a water-ice bath, and the temperature was kept constant by constantly adding ice around the reaction flask. As illustrated in Figure 8(a), although the amounts of produced hydrogen remained the same, 250 mL H_2 at all reaction temperatures, the elapsed time to produce the same amount of H_2 dramatically decreased with the increase in temperatures. The hydrolysis reaction of $NaBH_4$ was completed in about 2 min at 70 ºC, whereas it was completed in about 77 min at 0 ºC, as shown in the inset of Figure 8(a). The highest HGR and TOF vales were obtained for the hydrolysis reaction that occurred at 70 ^{0}C as 14501.16±1 (mL H_2) $(min)^{-1}$ (g of Metal)$^{-1}$and 34.25±1.2 (mol H_2) (mol catalyst $min)^{-1}$ as given Table 2. As the temperature increased the reaction rates, the increased HGR and TOF values with the increase in hydrolysis of $NaBH_4$ is expected [40-44]. The increase in reaction temperature leads to an increase in the reaction rates due to the increase number effective collisions with the reactants and catalyst. Therefore, the reaction rate of hydrogen generation increases with increase in the reaction temperature. The kinetic parameters of the hydrolysis reaction of $NaBH_4$ were calculated by using the very-well known Arrhenius (Eq. (4)) and Eyring (Eq. (5)) equations associated with the graphs ln k versus 1/T and ln (k/T) versus 1/T graphs [38,39].

$$\ln k = \ln A - (Ea/RT) \quad (4)$$

$$\ln (k/T) = \ln(kB/h) + (\Delta S\#/R) - (\Delta H\#/R)(1/T) \quad (5)$$

Here, k is the reaction rate constant and was calculated according to a zero-order kinetic expression, Ea is the activation energy, T is the absolute temperature, k_B is Boltzmann constant (1.381×10^{-23} J K^{-1}), h is Planck's constant (6.626×10^{-34} J.s), ΔH is activation enthalpy, ΔS is the entropy and R the gas is constant (8.314 J K-1 mol^{-1}). The kinetic parameters such as energy, enthalpy and entropy of cryogel p(AMPS)-Co composite systems were Ea=15.40±0.3 $kJmol^{-1}$, ΔH=12.85±0.2 $kJmol^{-1}$ and ΔS= -153.05±0.5 $Jmol^{-1}K^{-1}$, respectively. The activation energy values reported here for cryogel p(AMPS)-Co composite systems is one of lowest in comparison to conventional hydrogels [16,17 etc]. This value proves that cryogel p(AMPS)-Co composite systems can be very useful for catalytic applications.

3.6. The Reusability of p(AMPS)-Co Macroporous Composites

The reusability of porous p(AMPS)-Co composite catalyst systems was investigated by consecutively using them in the same hydrolysis reaction repeatedly. In brief, 0.1 g cryogel p(AMPS)-Co composite (containing 8.62 mg nanoparticles) was used in H_2 generation from $NaBH_4$ hydrolysis under the usual reaction conditions (50 mL 50 mM $NaBH_4$, 5 wt% NaOH content, at 30 ºC and 1000 rpm mixing rate). After the first use, p(AMPS)-Co metal composites were removed from the reaction medium, washed with plenty of water, and again placed into a similar fresh reaction medium under the same conditions and these steps were followed five times repetitively. As illustrated in Figure 9, there is no change in conversion of $NaBH_4$ for H_2 generation but its activity reduced from 100% to 82% at the end of the 5th use. The activity is calculated based on initial HGR to the HGRs of each use. The HGR and TOF values of p(AMPS)-

Co composite systems decreased to 2230 (mL H_2) $(min)^{-1}$ (g of M)$^{-1}$ and 5.26 (mol H_2) (mol catalyst min)$^{-1}$ from 2697 (mL H_2) $(min)^{-1}$ (g of M)$^{-1}$ and 6.37 (mol H_2) (mol catalyst min)$^{-1}$, respectively, at the end of 5th use as can be seen in Table 2. The mass loss of catalyst during catalytic reaction was not observed as the amounts of metal ions were determined before and after the hydrolysis reactions. However, due to the formation of $NaBO_2$ and its accumulation on the catalytic composite system, the activity decreased as we checked that there is no leakage or elution of metal nanoparticles from the cryo- and hydrogels networks [16, 40-44]. There are also similar results were reported in the literature that hydrogel-metal composites catalytic performances are reduced with repetitive uses. For example, the reusability of p(VPA), p(AAm-co-VSA) and p(SPM) were reported as about 15, 55, and 72%, respectively as reported earlier [18,43,44]. Therefore, it can be said that although there is a reduction in the activity of cryogel p(AMPS)-Co, they can be used successively with 100% conversion in H_2 production in $NaBH_4$.

Conclusions

Due to appealing properties such as excellent chemical stability, improved response rates and diffusion of solutes, super porous structure, and mechanical stability of cryogels, p(AMPS) cryogels were prepared and used as template for in situ metal nano particle preparation of Co and Ni and the resultant composites were used as catalyst media. Here, we have successfully demonstrated the use of macroporous cryogel p(AMPS)-Co composites in energy and environmental applications via H_2 generation from hydrolysis of $NaBH_4$, and reduction of toxic 4-NP to 4-AP, respectively.

The following conclusions and inferences can be deduced from this research:

• P(AMPS)-based superporous cryogels and conventional hydrogels were used in metal nanoparticle preparation of Co and Ni, as catalysis media for 4-NP reduction and in H_2 generation from hydrolysis of $NaBH_4$. It was found that Co nanoparticle-containing cryogel p(AMPS) provided better catalytic performances than its Ni nanoparticle-containing counterparts. The catalytic performances of Co-containing cryogel and conventional p(AMPS) hydrogels were compared in H_2 generation from hydrolysis of $NaBH_4$ and the cryogel p(AMPS)-Co composite exhibited superior catalytic performances.

• Kinetic parameters such as energy, enthalpy and entropy of superporous cryogel p(AMPS)-Co composite systems in H_2 generation from hydrolysis of $NaBH_4$ were calculated as Ea=15.40±0.3 kJmol^{-1}, ΔH=12.85±0.2 kJmol^{-1} and ΔS=-153.05±0.5 Jmol^{-1}K^{-1}. This activation energy is one of lowest Ea reported in the literature from similar studies.

• The superporous cryogel p(AMPS)-Co composite can also be used in various environmental applications such as nitro compound reduction and elimination of contamination by dyes, pesticides etc.

• Here, it can be summarized that cryogels with superporous structure can be used in many applications due to their added properties compared to smart or intelligent hydrogels.

Acknowledgements

This work is supported by the Scientific and Technological Research Council of Turkey (113T042) and (110T649).

Notes and references

[a] *Canakkale Onsekiz Mart University, Faculty of Sciences and Arts, Chemistry Department, 17100, Canakkale-Turkey. Address, Address, Town, Country. Fax: +90-2862181948; Tel: +90-2862180018-2041; E-mail sahiner71@gmail.com*

[b] *Nanoscience and Technology Research and Application Center (NANORAC), Terzioglu Campus. 17100, Canakkale-Turkey.*

References:

1 T.K. Zheleva and R. Ridolfi, *Energy,* 2006, **31**, 2486.
2 A.N. Ökte and D. Karamanis, *Appl. Catal.,B*, 2013, **142–143**, 538.
3 D-W. Zhuang, J-J. Zhang, H-B. Dai and P. Wang, *Int. J. Hydrogen Energy*, 2013, 38, 10845.
4 T. P. Bartkus, J. S. Tiena and C-J. Sung, Int. J. Hydrogen Energy, 2013, **38**, 4024.
5 H. Li, J. Liao, X. Zhang, W. Liao, L. Wen, J. Yang, H. Wang and R. Wang, *J. Power Sources* ,2013, **239**, 277.
6 A. Sartbaeva, V. L. Kuznetsov, S. A. Wells and P. P. Edwards, *Energy Environ. Sci.,* 2008, **1**,79.
7 J. Shen, Y. Zhang, X. Xu, C. Hua, X. Sun, J. Li, Y. Mu and L. Wang, *Water Res.*, 2013, **47**, 5511.
8 X-K. Kong, Z-Y. Sun, M. Chen, C-L. Chen and Q.-W. Chen, *Energy Environ. Sci.,* 2013, **6**, 3260.
9 M. H. Loghmani and A. F. Shojaei, *J. Alloys Compd*., 2013, **580**, 61.
10 Y. Guo, Q. Feng, Z. Dong and J. Ma, *J. Mol. Catal. A: Chem*., 2013, **378**, 273.
11 A. Chinnappan, H-C. Kang and H. Kim, *Energy*, 2011, **36**, 755.
12 H. Li, J. Liao, X. Zhang, W. Liao, L. Wen, J. Yang, H. Wang and R. Wang, *J. Power Sources*, 2013, **239**, 277.
13 N. Sahiner, H. Ozay, O. Ozay and N. Aktas, *Appl. Catal., B,* 2010, **101**, 137.
14 M. B. Romanello and M. M. Fidalgo de Cortalezzi, *Water Res.*, 2013, **47**, 3887.
15 M.D.W. Grogan, S.C. Heck, L.M. Xiao, R. England, S.A. Maier and T.A. Birks, *J. Non-Cryst. Solids*, 2012, **358**, 241.
16 N. Sahiner, *Prog. Polym. Sci.*, 2013, **38**, 1329.
17 N. Sahiner and A. O. Yasar, *Fuel Process. Technol*., 2013, **111**, 14.
18 N. Sahiner and S. Sagbas, *Colloids Surf*., A, 2013, **418**, 76.
19 S. Reichelt, A. Prager, C. Abe and W. Knolle, *Radiat. Phys. Chem*., 2014, **94**, 40.
20 V. Stoyneva, D. Momekova, B. Kostova and P. Petrov, *Carbohydr. Polym*., 2014, **99**, 825.
21 P. Karacan and O. Okay, *React. Funct. Polym*., 2013, **73**, 442.
22 S. T. Koshy, T. C. Ferrante, S. A. Lewin and D. J. Mooney, *Biomaterials*, 2014, **35**, 2477.
23 B. Kostova, D. Momekova, P. Petrov, G. Momekov, N. Toncheva-Moncheva, C. B. Tsvetanov and N. Lambov, *Polymer*, 2011, **52**, 1217.
24 P. Petrova, A. Utrata-Wesołek, B. Trzebicka, C. B. Tsvetanova, A. Dworak, J. Aniol and A. Sieron, *Eur. Polym. J*., 2011, **47**, 981.
25 S. Zheng, T. Wang, D. Liu, X. Liu, C. Wang and Z. Tong, *Polymer*, 2013, **54**, 1846.
26 K-H. Chang, H-T. Liao and J-P. Chen, *Acta Biomater*., 2013, **9**, 9012.
27 P. Petrov, E. Petrova, B. Tchorbanov and C. B. Tsvetanov, *Polymer*, 2007, **48**, 4943.
28 M. B. Dainiak, I. U. Allan, I.. N. Savina, L. Cornelio, E. S. James, S. L. James, S. V. Mikhalovsky, H. Jungvid and I. Y. Galaev, *Biomaterials*, 2010, **31**, 67.
29 V.M. Gunkoa, V.V. Turov, V.I. Zarko, E.M. Pakhlov, G.P. Prykhodko, O.S. Remeza, R. Leboda, J. Skubiszewska-Ziebab and J.P. Blitz, *Colloids Surf., A*, 2013, **436**, 618.
30 V. I. Lozinsky, I. Y. Galaev, F. M. Plieva, I. N. Savina, H. Jungvid and B. Mattiasson, *Trends Biotechnol.*, 2003, **21**, 445.
31 M. M. Ozmen and O. Okay, *Polymer*, 2005, **46**, 8119.
32 B. Akduman, M. Uygun, D. A. Uygun, S. Akgöl and A. Denizli, *Mater. Sci. Eng., C*, 2013, **33**, 4842.
33 N. Bereli, D. Türkmen, K. Köse and A. Denizli, *Mater. Sci. Eng., C*, 2012, **32**, 2052.
34 K. Tekin, L. Uzun, C. A. Sahin, S. Bektas, A. Denizli, *React. Funct. Polym.*, 2011, **71**, 985.

35 N. Bereli, G. Sener, E. B. Altıntas, H. Yavuz, A. Denizli, *Mater. Sci. Eng., C*, 2010, **30**, 323.
36 L. Ai and J. Jiang, *Bioresour. Technol.*, 2013, **132**, 374.
37 J.C. Walter, A. Zurawski, D. Montgomery, M. Thornburg and S. Revankar, *J. Power Sources*, 2008, **179**, 335.
38 D. Xu, P. Dai, X. Liu, C. Cao and Q. Guo, *J. Power Sources*, 2008, **182**, 616.
39 A-J. Hung, S-F. Tsai, Y-Y. Hsu, J-R. Ku, Y-H. Chen and C-C. Yu, *Int. J. Hydrogen Energy*, 2008, **33**, 6205.
40 N. Sahiner, S Butun, T. Turhan, *Chem Eng Sci,* 2012, **82**, 114.
41 S. Sagbas, N. Sahiner, *Fuel Process. Tech*., 2012, **104**, 31.
42 T. Turhan, Y.G. Avcibasi, N. Sahiner, *J. Indust. Eng, Chem*., 2013, **19**, 1218.
43 F. Seven, N. Sahiner, *Int. J. Hydrogen Energy*, 2013, **38**, 777.
44 T. Turhan, T.G. Avcibasi, N. Sahiner, *Energy*, 2013, **55**, 511.

Figure Caption

Figure 1. The polymerization mechanism of p(AMPS) cryogels **(a)**, and the visual demonstration of the swelling of 0.1% crosslinked p(AMPS) hydrogels **(b)**, and **(c)** 10% crosslinked p(AMPS) cryogels. The optical microscope **(d),** and **(e)** SEM images of p(AMPS) cryogels.

Figure 2. The SEM images of p(AMPS) cryogels under **(a)** 50, **(b)** 150, **(c)** 370, and **(d)** 400 magnification, and the optical microscope images of p(AMPS) cryogels under **(e)** 10X and **(f)** 20X magnifications.

Figure 3. (a) The reduction of Co(II) ions to cobalt nanoparticles within cryogel matrices, and **(b)** TEM images of cobalt nanoparticles within porous cryogel networks.

Figure 4. (a) Metal ion absorption capacities of p(AMPS) hydrogel and cryogel, and **(b)** TGA thermogram of p(AMPS) hydrogel, cryogel and their metal nanoparticle-containing composites.

Figure 5. (a) Reaction mechanisms of H_2 generation from hydrolysis of $NaBH_4$, and reduction of 4-NP. **(b)** H_2 generation from hydrolysis of $NaBH_4$ via ferrite-containing 0.1 g p(AMPS)-Co metal nanoparticles (8.71 mg nanoparticles) and magnetic three times Co(II) loaded-reduced 0.1 g p(AMPS)-Co (19.54 mg/g nanoparticles) catalyst system under externally applied magnetic field. [Reaction conditions: 50 mL 50 mM $NaBH_4$, 5 wt% NaOH, 30 °C, 1000 rpm mixing rate.] **(c)** UV–Vis spectra of 4-NP reduction to 4-AP by using 0.1 g p(AMPS)-Co cryogel composite catalyst systems (8.62 mg Co nanoparticles) [Reaction conditions: 50 mL 0.01 M 4-NP, 0.28 M $NaBH_4$, 30 ºC, 1000 rpm mixing rate].

Figure 6. (a) H_2 generation from hydrolysis of 50 mL 50 mM $NaBH_4$ via 8.62 mg Co nanoparticle-containing 0.1 g cryogel p(AMPS)-Co composite, and 0.069 g hydrogel p(AMPS)-Co composites. [Reaction conditions: 50 mL 50 mM $NaBH_4$, 5 wt% NaOH, 30 °C, 1000 rpm.] **(b)** H_2 generation from hydrolysis of $NaBH_4$ via 0.1 g cryogel p(AMPS)-Co (8.62 mg Co nanoparticles) and 0.1 g p(AMPS)-Ni composites (8.94 mg Ni nanoparticles). [Reaction conditions: 50 mL 50 mM $NaBH_4$, 5 wt% NaOH, 30 °C, 1000 rpm.]

Figure 7. (a) The effect of pH and **(b)** the effect of water type on H_2 generation reaction from hydrolysis of sodium borohydride via 0.1 g cryogel p(AMPS)-Co (8.62 mg nanoparticles). [Reaction conditions: 50 mL 50 mM $NaBH_4$, 5 wt% NaOH, 30 °C, 1000 rpm].

Figure 8. (a) The effect of temperature on the hydrolysis of $NaBH_4$, **(b)**, ln k versus 1/T (Arrhenius eq.), and **(c)**, ln (k/T) versus 1/T (Eyring eq.) [Reaction Conditions: 50 mL 50 mM $NaBH_4$, 5 wt% NaOH, 1000 rpm, 8.62 mg Co nanoparticles in 0.1 g cryogel p(AMPS)-Co composite].

Figure 9. The activity and the conversion ability of the cryogel p(AMPS)-Co composite for repetitive $NaBH_4$ hydrolysis [Reaction conditions: 50 mL 50 mM $NaBH_4$, 5 wt% NaOH, 30 °C, 1000 rpm, 8.62 mg Co nanoparticle in 0.1 g cryogel].

Table Legend

Table 1. The amount of metal nanoparticles, TGA results, TOF (turn over frequency) values and hydrogen generation rates (HGR) of various catalyst systems.

Table 2. The change in TOF and HGR values of cryogel p(AMPS)-Co metal composites (8.62 mg particles) depending on different reaction conditions.

5